

1 LINKING THE HIGH-RESOLUTION ARCHITECTURE OF MODERN AND ANCIENT  
2 WAVE-DOMINATED DELTAS: PROCESSES, PRODUCTS AND FORCING FACTORS  
3 **R. Bruce Ainsworth<sup>1</sup>, Boyan K. Vakarelov<sup>2</sup>, Christian H. Eide<sup>3</sup>, John A. Howell<sup>4</sup> and Julien**  
4 **Bourget<sup>5</sup>**

5 *<sup>1</sup>Australian School of Petroleum, University of Adelaide, Adelaide, SA 5005, Australia*

6 *<sup>2</sup>SEDBASE OOD, 21B Moskovska Street, Sofia 1000, Bulgaria*

7 *<sup>3</sup>Department of Earth Science, University of Bergen, PO Box 7803, 5020 Bergen, Norway*

8 *<sup>4</sup>School of Geosciences, University of Aberdeen, Meston Building, Aberdeen, AB24 3UE, UK*

9 *<sup>5</sup>Centre for Energy Geoscience, School of Earth Sciences, University of Western Australia,*  
10 *Crawley, WA 6009, Australia*

11 **ABSTRACT:** Wave-dominated deltas are often fed by single trunk distributary channels which  
12 can remain the primary source of sediment supply to the delta for periods of thousands of years.  
13 Consequently, the sedimentary architecture of the delta can record subtle changes in sediment  
14 supply and wave intensity over significant periods of time. The geomorphological expression of  
15 these variations are beach-ridge elements and disconformity-bounded, beach-ridge element-sets.  
16 There are two types of beach-ridge element-sets observed on modern deltas, those associated  
17 with mouth-bar progradation (mouth-bar element sets), and those associated with delta-lobe  
18 flank accretion (lobe element-sets). When the ratio of the rate of sediment supply by the fluvial  
19 system (F) is relatively high with respect to the rate of sediment removal at the mouth-bar  
20 location by waves (W) (i.e., the F/W ratio is high), the mouth-bar element-sets are deposited.  
21 When the F/W ratio is low, sediment is preferentially transported to the lobe flanks and the lobe  
22 element-sets are deposited. The mouth-bar and lobe element-sets are bounded by the same  
23 unconformity and disconformity surfaces and are together termed element-set pairs. Analogous  
24 cyclical patterns of deposition have also been recognized in plan-view and vertical sections from



50 unlikely given the variability in formative durations of individual beach ridges since some have  
51 decadal and others have centennial-scale durations (Sanjaume and Tolgensbakk, 2009). The  
52 grouping of ridges into disconformity-bounded beach-ridge sets is also a common feature on  
53 wave-dominated deltas and coastlines (Fig. 1). The bounding surfaces of beach-ridge sets are  
54 typically ascribed to reductions in sediment supply to the shoreline (Tamura, 2012) leading to  
55 coastal erosion by waves and the formation of beach ridge unconformity and disconformity  
56 surfaces. Renewed sedimentation results in the initiation of a new beach-ridge set (Tamura,  
57 2012).

58         Cyclical groupings of depositional beds and bedsets, and stratal disconformities have also  
59 been described in vertical sections in ancient wave-dominated deltaic deposits (e.g. Hampson,  
60 2000; Sømme et al., 2008). Some authors have attempted to relate these stratal units and  
61 disconformities to those observed in modern systems (Hampson and Storms, 2003; Storms and  
62 Hampson, 2005, Hampson et al., 2008; Sømme et al., 2008). Two-dimensional forward-  
63 modeling testing key uncertainties such as changes in sediment supply, wave power, and sea  
64 level (Storms and Hampson, 2005, Sømme et al., 2008; Charvin et al., 2011) have been able to  
65 replicate similar stratal geometries to those observed, and suggest that these processes  
66 individually, or in conjunction with each other, may be responsible for the formation of beach  
67 ridges and beach-ridge sets.

68         Recent advances in the classification of shallow marine systems (Ainsworth et al. 2011;  
69 Vakarelov and Ainsworth, 2013; Ainsworth et al. 2017) have enabled both modern and ancient  
70 architectural units from bed-scale up to deposystem-scale to be recognized and classified. This  
71 consistent classification enables direct cross-comparison of modern and ancient systems at the  
72 same architectural-unit scales (Table 1). This permits measured timeframes for architectural units  
73 from modern dated coastal systems (Carbon 14 [ $^{14}\text{C}$ ] or optically stimulated luminescence

74 [OSL]; see examples in Tamura, 2012) to be applied as time duration estimates for the same  
75 stratigraphic units in ancient deposystems (c.f. Miall, 2015).

76 Rivers that supply the same wave-dominated delta lobe for hundreds to thousands of  
77 years (Fig. 1) provide a quasi-continuous record of sediment supply to the river mouth. This  
78 permits patterns or cycles in sediment supply that may exist on a seasonal, decadal or centennial  
79 time-scale to be identified via mapping and dating of beds, beach ridges and beach-ridge set  
80 bounding surfaces.

81 The key objectives of this paper are: 1) to compare the stratal patterns of beach ridges and  
82 beach-ridge sets in well-constrained and dated Holocene, wave-dominated, fluvial-influenced  
83 deltas (Wf classification of Ainsworth et al. 2011) with those from ancient Wf deltaic systems,  
84 and 2) to propose possible formative driving mechanisms for the cyclical changes in beach-  
85 ridge-set packaging to explain the observed stratal patterns. The genesis of non-deltaic, wave-  
86 dominated, beach-ridge strandplains are not considered in this paper.

## 87 **ARCHITECTURAL OBSERVATIONS ON WAVE-DOMINATED DELTAS**

### 88 *Architectural Terminology for Comparing Modern and Ancient Systems*

89 In order to provide a mechanism for identifying equivalent stratigraphic units from  
90 horizontal sections (usually satellite imagery of modern systems and high-resolution seismic  
91 attribute data from ancient systems) with the same architectural units in vertical sections (usually  
92 ancient systems in outcrop sections or modern and ancient systems in well logs and cores),  
93 Vakarelov and Ainsworth (2013) developed an architectural hierarchy called the *WAVE*  
94 classification (Table 1). Figure 2 details the horizontal (Figs. 2A, B) and vertical expression (Fig.  
95 2C) of the architectural units pertinent to describing the level of detail observed in modern wave-  
96 dominated delta lobes (Fig. 1; Table 1). The individual wave-dominated delta lobe formed by a  
97 discrete fluvial avulsion is termed an element complex set (ECS; Figs. 1-2; Table 1; Vakarelov  
98 and Ainsworth, 2013; Ainsworth et al., 2017). The ECS is subdivided into elements (beach-ridge



99 elements) and element sets (beach-ridge element-sets; Figs. 1-2; Table 1). There are two types of  
100 beach-ridge element-sets observed on the modern delta shown in Figure 1, those associated with  
101 mouth-bar progradation (mouth-bar element-sets; shaded green in Figs. 1-2; Table 1), and those  
102 associated with delta-lobe flank accretion (lobe element-sets; shaded orange in Figs. 1-2; Table  
103 1). The two element-set types can be seen to regularly alternate close to the river mouth location  
104 and form mouth-bar and lobe element-set pairs which are bounded by erosional unconformities  
105 to non-depositional unconformities (Figs. 1-2). This alternating mouth-bar then lobe depositional  
106 cyclicity has been well documented by Rodriguez et al. (2000) and Bhattacharya and Giosan  
107 (2003). The unconformities are most easily observed at the river-mouth location and suggest  
108 periods where the ratio of the rate of sediment supply by the river ( $F$ ) is relatively low with  
109 respect to the rate of sediment removal at the mouth-bar location by waves ( $W$ ). That is, the  $F/W$   
110 ratio is relatively low. The unconformities pass laterally into non-depositional unconformities  
111 that form on the flanks of the delta in the lobe locations at times when active deposition is  
112 primarily occurring on the mouth-bar at the river mouth during periods of high  $F/W$  (Figs. 1-2).

113 For completeness, the *WAVE* classification terminology for larger scale architectural  
114 units is also summarized in Table 1. An element-complex is a genetically-related group of  
115 elements, element-sets and element-set pairs formed in the same depositional sub-environment  
116 (e.g. a mouth-bar or a delta lobe; Fig. 2B). Genetically related groups of element-complexes  
117 form element-complex sets (ECS; delta lobes). Groups of ECS units generated by the same river  
118 under the same coastal process regime are termed element-complex assemblages (ECA;  
119 equivalent to a modern-day, wave-dominated delta). The deposits of a regressive transit of  
120 deposystems (multiple coeval deltas and adjacent coastlines) across a shelf are termed regressive  
121 element-complex-assemblage sets (RECAS). The overlying deposits of the transgressive transit  
122 of deposystems across the shelf are called transgressive element-complex-assemblage sets  
123 (TECAS). The composite regressive and transgressive stratigraphic-unit bounded by

124 transgressive surfaces is the regressive-transgressive sequence (RT sequence or RTS). This level  
125 of hierarchy is the preferred level for the term “parasequence” (PS) when using the *WAVE*  
126 classification terminology (e.g. Ainsworth et al. 2018; this paper). The parasequence term is also  
127 used at this hierarchical level in the classical Book Cliffs papers (e.g. Hampson, 2000; Hampson  
128 et al. 2012). Note that each level of architecture from element- to ECA-scale can also be assigned  
129 a process classification prefix descriptor, e.g. Wft mouth-bar EC (Fig. 3; Ainsworth et al. 2011;  
130 Vakarelov and Ainsworth, 2013).

131       Following Walther’s Law, architectural units recognized in plan views (beach-ridge  
132 elements, beach-ridge element-sets and delta lobes) should also have an equivalent expression in  
133 vertical sections (Table 1). Ainsworth et al. (2017) detailed the stacking patterns that define the  
134 different architectural units in vertical sections for different types of deltaic systems. Figure 2C  
135 illustrates that in symmetrical wave-dominated deltas, the beach-ridge elements are represented  
136 by bedsets (Table 1). Bedsets have been defined as dm-to-m scale sets of genetically related beds  
137 (Ainsworth et al. 2017). They can be arranged in an upward-thickening and coarsening or  
138 upward-thinning and fining trend. In normally prograding, wave-dominated systems, subsequent  
139 elements thicken-upward to form element-sets which are the vertical equivalent of beach-ridge-  
140 sets observed in plan-view (Table 1). In vertical sections, breaks in upward-thickening element  
141 trends define element-set boundaries. The element-sets themselves then thicken-upward to form  
142 element-complex sets (Fig. 2C). Breaks in upward-thickening element-set trends define element-  
143 complex-set boundaries (ECS; Ainsworth et al. 2017). This is a result of the lateral offset of  
144 subsequent avulsion-related ECS (delta lobes) resulting in a thinning of the younger element-set  
145 belonging to the new ECS.

#### 146                   *Holocene to Modern Wave-Dominated Deltas*

147       The beach ridge and beach-ridge set architecture of Holocene to modern wave-dominated  
148 deltas are well illustrated by the Usumacinta–Grijalva Delta (Mexico; Fig. 1, Table 2). This delta

149 has been the subject of detailed studies by numerous authors. See the recent paper by Nooren et  
150 al. (2017) and references therein for other relevant work. The current active lobe (ECS) of the  
151 delta initiated with the avulsion of the Usumacinta river circa 970 years before present (Fig.1;  
152 Nooren et al. 2017). The delta shows well developed beach ridges which group into beach-ridge  
153 sets around the mouth of the river (mouth-bar beach-ridge sets), and beach-ridge-sets away from  
154 the mouth of the river on the flanks of the delta in the lobe areas (lobe beach-ridge sets). The  
155 beach-ridge sets around the river mouth formed during periods of high fluvial-discharge relative  
156 to the power of the waves to redistribute the sediment (high F/W time periods). Whilst the beach-  
157 ridge sets on the lobes formed during periods of low fluvial-discharge relative to the power of the  
158 waves to redistribute the sediment (low F/W time periods). Sediment was thus eroded from the  
159 mouth bar areas and transported to the lobe flanks in what is here termed the “lobe healing-  
160 phase” (Fig. 2A). The beach-ridge sets of the mouth bars (high F/W) and lobes (low F/W) are  
161 grouped together by unconformity and disconformity surfaces and form high and low F/W  
162 beach-ridge element-set pairs (Figs. 1-2).

163 An example of a vertical section through a Holocene, wave-dominated, mouth-bar  
164 deposit can be seen in Fig. 3. This core is from the Mitchell River Delta, Gulf of Carpentaria,  
165 Queensland, Australia. See Nanson et al. (2013), Lane (2016) and Lane et al. (2017) for details  
166 of the Holocene evolution of the Mitchell River Delta. The vertical stratigraphic patterns  
167 depicted in the schematic mouth-bar deposits in Fig. 2C can be readily observed in the Mitchell  
168 Delta mouth-bar (Fig. 3). In the core, the upward-thickening groups of elements form element-  
169 sets. Element-complex set (delta lobe) boundaries are defined when upward-thickening element-  
170 set trends are broken (Ainsworth et al. 2017). Note that these element, element set and element-  
171 complex set surfaces can sometimes have little or no definitive sedimentological expression in  
172 individual cores. In these cases, recognition of these surfaces thus relies on the stacking pattern  
173 trends detailed above (Fig. 2; Ainsworth et al. 2017).

174

*Ancient Wave-Dominated Deltas*

175

176

177

178

179

180

181

182

183

184

185

The physical recognition of sub-aerial beach-ridge (element) and beach-ridge-set (element set) deposits in ancient progradational wave-dominated deltas is more challenging than for the Holocene deltas given the potential for the beach ridges (if originally present) to be removed during subsequent transgressive erosion events. The most convincing evidence of ancient beach-ridge deposits are examples from 3D seismic-attribute data, which can provide images of plan-view sections through beach-ridge fields. An excellent example from the Jurassic of the North Sea was provided by Jackson et al. (2010). A higher-resolution seismic example which delineates beach ridges, high and low F/W beach-ridge element-sets and beach-ridge element-set pairs can be seen in Figure 4. This example is from the late Miocene, Bare Formation from the Northwest Shelf of Australia. See Sanchez et al. (2012) for details on the regional setting of the Bare Formation.

186

187

188

189

190

191

192

193

194

195

The link between the critical architectural units of a wave-dominated delta in plan-view (modern and seismic attribute data) and their vertical equivalents (well, core and outcrop data) is shown schematically in Figure 2 and from a real example in Figure 5 from a wave-dominated delta in the Eocene, Mangahewa Formation of the Taranaki Basin, New Zealand. See Higgs et al. (2012) for details on the regional setting of the Mangahewa Formation. Figure 5 shows an example of beach ridges in plan-view seismic-attribute data which are tied to vertical core and wireline log data, which also exhibit the element and element-set cyclicity detailed in Figure 2. The beach ridges themselves are imaged on the seismic due to the peat accumulations (which compact over time to become coals) in the swales between the ridges which exhibit as low impedance intervals on the seismic data.

196

197

198

There are relatively few reports of the physical expression of beach ridges being identified and described from outcrops. A notable exception is the interpreted beach ridge deposits from the Campanian of the Alberta Basin, Canada (Ainsworth et al. 2015). Since direct

199 identification of the beach-ridge, beach-ridge-set and delta-lobe equivalents in vertical sections is  
200 challenging, recognition generally relies on the identification of architectural unit stacking  
201 patterns as defined in Figure 2C (c.f. Ainsworth et al. 2017).

202         The Blackhawk Formation and Star Point Sandstone of the Book Cliffs and Wasatch  
203 Plateau, Utah, USA comprise well documented extensive outcrops of Upper Cretaceous, wave-  
204 dominated deltaic systems (for a summary see Hampson and Howell, 2005). These well-studied  
205 outcrops provide an ideal location to examine vertical stacking patterns of stratal units deposited  
206 by wave-dominated deltas. An example from helicopter lidar derived virtual outcrops from the  
207 Sunnyside Member of the Blackhawk Formation, Book Cliffs, Utah is shown in Figure 6. See  
208 Sømme et al. (2008) and Eide et al. (2015) for a summary of the stratal architecture of the  
209 Sunnyside Member. The interpreted photo panel in Figure 6B illustrates the hierarchy of stratal  
210 packages from the smallest bedsets (elements), the groupings of upward-thickening elements into  
211 element sets, and the groupings of upward-thickening element-sets into element-complex sets.  
212 Breaks in upward-thickening trends define stratal unit boundaries. The element-complex sets  
213 stack vertically to form the parasequences.

214         The KSP010 parasequence of the Star Point Sandstone, Wasatch Plateau, Utah, USA  
215 (Eide et al. 2014) provides another example of the vertical stratal unit stacking hierarchy from a  
216 wave-dominated delta (Figs. 7, 8). This example also provides vertical detail from the mouth-bar  
217 to lobe transition area (Fig. 7) where the detailed onlap and downlap relationships of element-  
218 set-pairs can be observed directly adjacent to the distributary channel that fed the delta. The  
219 detailed vertical architecture of the lobe element-complex section of the parasequence is  
220 illustrated by bed-scale sedimentary logging (Fig. 8B) and comprises genetically related sandier  
221 and thickening-upward beds grouped into bedsets (elements). These elements are themselves  
222 grouped into sandier and thickening-upward genetically related units (element sets). The element  
223 sets then group into sandier and thickening-upward units (element complex sets). The element-

224 complex-sets have been equated to deltaic lobe-switching events (Eide et al. 2014; Ainsworth et  
225 al. 2017). This lobe switching relationship can also be observed in vertical section on the  
226 summary section derived from the helicopter lidar panel in Figure 8A.

## 227 DISCUSSION

### 228 **Linking Modern and Ancient Wave-Dominated Deltas**

229 Previous authors have attempted to link the cyclicity observed in wave-dominated deltas  
230 interpreted from outcrop logs to the cyclicity seen in modern wave-dominated delta systems  
231 (Hampson and Storms, 2003; Storms and Hampson, 2005, Hampson et al. 2008; Sømme et al.  
232 2008; Charvin et al. 2010). However, no rules for identification of architectural units in vertical  
233 section were presented by these authors. The term “bedset” in the Blackhawk Formation, Utah,  
234 USA studies listed above has been equated to the avulsion body or delta lobe by some of the  
235 workers and this concurs with our interpretation of the element-complex set (Figs. 1-8; Table 1;  
236 Vakarelov and Ainsworth, 2013; Ainsworth et al. 2017). An advance presented here over the  
237 previous work is the recognition of two further levels of stratal unit hierarchy, at a scale below  
238 that of the delta-lobe body (ECS): 1) the element (“bedset” *sensu* Ainsworth et al. 2017; Table 1)  
239 which is suggested to correspond to the “beach-ridge” observed in plan-view on modern delta  
240 systems (Figs. 1-2, Table 1) and on high-resolution seismic attribute data (Figs. 4-5), and 2) the  
241 element-set, which is suggested to correspond to the “beach-ridge sets” (Table 1) observed in  
242 plan-view on modern systems (Fig. 1) and on high-resolution seismic attribute data (Fig. 4).

243 Figures 8C and 8D illustrate a model for linking the cyclicity observed on modern wave-  
244 dominated deltas (Figs. 1, 3) with that observed on ancient deltas (Figs. 4 - 8). Breaks in the  
245 upward-thickening trends of elements define element-set boundaries and breaks in the upward  
246 thickening trends of element sets define element-complex set or fluvial-avulsion boundaries  
247 (Ainsworth et al., 2017). The fluvial avulsion event in Fig. 8C results in the deposition of a new  
248 delta lobe (ECS-2). In vertical section, the new delta lobe (ECS-2) is recognized by the break in

249 the expected upward-thickening stacking patterns of the element sets and the overlying minor  
250 flooding surface (Fig. 8D).

### 251 **Importance of Element, Element Set and Element-Complex Set Surfaces**

252 Given the cryptic sedimentological expression of some of the element, element set and  
253 element-complex set stratigraphic surfaces in core and on wireline data (Figs. 3, 5-8), the ability  
254 to identify the hierarchical scale of the stratigraphic surface from the stacking pattern rules  
255 described in this paper is critical for reservoir characterization purposes. Each of these three  
256 types of surfaces are represented in cross-sectional view by clinofolds (Fig. 8D). Since the three  
257 different hierarchical scales of surfaces all represent breaks in sand deposition and are draped by  
258 shales, they all represent potential barriers or baffles to fluid flow in hydrocarbon or hydrological  
259 reservoirs (e.g. Ainsworth et al. 1999; Sech et al. 2009; Graham et al. 2015). The hierarchical  
260 stratigraphic significance of the clinofolds is also most likely directly related to their lateral  
261 extent and hence their ability to impact fluid flow within a reservoir. Element-scale clinofolds  
262 are likely to be the least areally extensive and hence the least impactful in terms of fluid flow but  
263 will be more numerous (Fig. 8D). Element-complex set, avulsion-lobe abandonment scale  
264 clinofolds are likely to be more laterally extensive and hence more impactful on fluid flow but  
265 the least numerous type of surface (Fig. 8D). Element-set scale clinofolds will be of  
266 intermediate importance (Fig. 8D). More quantitative data is required on each of the three types  
267 type of stratigraphic clinofold surface to accurately characterize them in terms of ranges of  
268 frequency of occurrence and lateral extents.

### 269 **Depositional Rates**

270 Towards the mouth of the river, where the stratigraphic record is most sensitive to fluvial  
271 input rates, individual beds represent daily or seasonal activity (Table 3) whilst elements  
272 (individual beach-ridges and bedsets) represent the product of multiple storm and river flood  
273 events and can be initiated by autogenic processes such as decadal-scale fluvial-discharge cycles

274 (Rodriguez et al. 2000) or fairweather progradation of beach berms (Tamura, 2012; Table 3).  
275 Individual river flood events can vary in intensity. For example, once in a decade and once in a  
276 century scale floods will be higher discharge events than annual floods. The resultant deposits of  
277 these types of events are hence predicted to be thicker and more extensive individual event beds  
278 than the annual flood event beds. The genesis of the element-sets and element-set-pairs detailed  
279 from modern and ancient examples in this paper, have not been the subject of previous  
280 speculation or discussion. Carbon 14 and OSL dating of modern deltas (Fig. 1; Table 2) suggest  
281 that the element-set-pairs of mouth-bar beach-ridge sets and lobe beach-ridge sets, which are  
282 related to high and low F/W cycles respectively, occur over centennial time-scales (Fig. 9;  
283 Tables 2-3).

284 Further from the river mouth on the flanks of the delta lobes (e.g. see location ii on Fig.  
285 1C), sediment accumulation rates are slower (only 2.5 km of progradation compared to 6.7 km of  
286 progradation at the river mouth on the Usumacinta-Grijalva Delta; Fig. 1), mouth-bar element  
287 sets are not deposited and there are also fewer beach ridges on the lobe than at the river mouth.  
288 These relationships are also detailed schematically in Figure 9. The obvious stratigraphic  
289 unconformities defining the element sets at the river mouth are less obvious at the lobe locations  
290 and in some places appear concordant with older strata (disconformities). The result of this is  
291 that there are fewer beach ridges on the lobe flanks representing the same number of beach  
292 ridges and the same amount of time at the river mouth (Fig. 9C). That is, if beach ridge duration  
293 is calculated by dividing the time taken for deposition by the number of beach ridges (a common  
294 method for estimating beach-ridge durations), then individual beach ridges on the lobes appear to  
295 represent greater amounts of time than beach ridges at the river mouth (Fig. 9C). However, in the  
296 case of wave-dominated deltas, this apparent mismatch in beach-ridge duration calculations is  
297 likely to be a function of the time sequestered in the unconformities and disconformities (Fig.



298 9D, E) rather than being due to significant differences in the actual time taken to deposit an  
299 individual beach ridge.

### 300 **The Impact of Real World Delta Complexity**

301 The models detailed in Figures 2, 8C, 8D and 9 represent the simplest form of a  
302 symmetric wave-dominated delta, wherein all the sediment supplied to the delta is delivered by  
303 the river and redistributed at the river mouth by waves. In the case of the Usumacinta–Grijalva  
304 Delta (Fig. 1), sediment supply to the delta through the trunk distributary channel was basically  
305 uninterrupted for the past circa 970 years (Nooren et al. 2017). In other Wf symmetrical deltas,  
306 such as the Jequitinhonha Delta (Brazil), constant sediment supply was not maintained along the  
307 axis of the one trunk distributary channel for the duration of the current delta lobe (ECS; Fig. 10,  
308 Table 2). The Jequitinhonha Delta has previously been described by Dominguez et al. (1983,  
309 1987) and Martin et al. (1983). It is currently undergoing forced regression (Martin et al. 2003;  
310 Dias and Kjerfve, 2013). The active lobe of the Jequitinhonha delta initiated with the avulsion of  
311 the Jequitinhonha river circa 2,500 years before present (Fig. 10; Martin et al. 1993). The current  
312 delta lobe at the river mouth location has prograded 8 km in the last 2,500 years (Fig. 10C). The  
313 geomorphology of the delta suggests that during this time the main channel has also diverted to  
314 the north for periods of time and then back to the current distributary channel location (Fig.  
315 10C). This may indicate that the count of element-set pairs along the main distributary channel  
316 (Fig. 10C; Table 2) is incomplete and may represent a minimum number.

317 In many modern deltas, sediment is also supplied to the system from other sources, apart  
318 from the deltaic distributary-channels, namely by longshore-transport mechanisms. Some deltas  
319 exhibit a strong degree of longshore sediment-supply. See Bhattacharya and Giosan (2003) for a  
320 summary of the impact of out-of-plane longshore sediment transport on delta morphology.

321 Consequently, the models proposed herein would require modification to account for varying

322 degrees of longshore transport supplying sediment to the delta from sources external to the deltas  
323 own distributary channel(s).

324         The Paraiba do Sul Delta (Brazil) (Fig. 11, Table 2) is a well-documented asymmetrical  
325 Wf delta and has been the subject of work by multiple previous authors (e.g. Dominguez et al.  
326 1983, 1987; Martin et al. 1985, 1993, 2003; Da Rocha, 2013; Vasconcelos et al. 2015). For the  
327 past 5,000 years it has been undergoing forced regression (Martin et al. 1985, 1993, 2003; Dias  
328 and Kjerfve, 2013). The current active lobe of the Paraiba do Sul delta initiated with the avulsion  
329 of the Paraiba do Sul river. The timing of this event varies depending on the type of age dating  
330 method utilized (Table 2). Martin et al. (1993) using  $^{14}\text{C}$  methods date the avulsion at circa 2,500  
331 years before present. However, Vasconcelos et al. (2016) using OSL methods date the avulsion  
332 at circa 1,300 years before present. The current delta lobe at the river mouth location has thus  
333 prograded 11 km in the last 1,300 to 2,500 years (Fig. 11C). In this example, there is no  
334 representation of mouth bar deposits on the updrift side of the delta, since the mouth-bars are  
335 deflected downdrift by longshore currents. However, the updrift part of the delta, the lobe EC is  
336 still segmented into an active mouth-bar progradation phase of beach ridges (high F/W) and a  
337 delta-lobe healing phase (low F/W) as per the deposits of the symmetric deltas of the  
338 Usumacinta–Grijalva and Jequitinhonha Deltas detailed in Figures 1 and 10 respectively. In the  
339 Paraiba do Sul Delta, both the high and low F/W lobe element-sets are accreting due to sediment  
340 supplied from older eroding delta lobes to the south (Fig. 11).

341         Note that the asymmetrical Paraiba do Sul delta has high and low F/W element-set pairs  
342 formed on the same centennial scale cyclicity as observed for the high and low F/W element-set  
343 pairs on the symmetrical deltas of the Usumacinta–Grijalva and Jequitinhonha (Table 2).

#### 344                 **Potential Forcing Mechanism of Centennial-Scale Stratigraphic Cycles**

345         The data discussed above suggests that beach-ridge element-sets near the river mouths of  
346 wave-dominated deltas represent periods of high F/W (Fig. 9D), and the beach-ridge element-

347 sets on the down-flank lobes represent delta-lobe healing during periods of low F/W (Fig. 9E).  
348 Together, the high and low F/W beach-ridge element-sets form beach-ridge element-set pairs.  
349 The unconformities and disconformities that separate the element-set pairs are diachronous,  
350 occurring in different locations at different times during a high to low F/W cycle (Figs. 9D, E).  
351 The element-set pairs are deposited on a centennial timescale, i.e., in the order of 100 to 200  
352 years (Table 2; Fig. 9). The repetitive changes in the F/W ratio required to form the element set  
353 pairs is a product of either regularly fluctuating sediment discharge from the river and/or  
354 regularly alternating wave energy.

355         The centennial-scale cyclicity forming the high and low F/W element-set pairs, that  
356 occurs over periods of thousands of years, from the three different modern deltas illustrated in  
357 this paper (Table 2), suggests that a regular external forcing factor could be responsible for  
358 producing this cyclicity. Possible centennial-scale climatic variations influencing precipitation  
359 rates have been postulated using computer modeling studies by Karnauskas et al. (2012).  
360 Greenland temperature records and lake levels in north-eastern USA have also been shown to  
361 illustrate centennial-scale climatic variability through the Holocene (Fawcett et al. 2011; Newby  
362 et al., 2014) as have sea surface temperatures in the early Holocene record of the Gulf of Mexico  
363 (LoDico et al. 2006). The studies of Thirumalai et al. (2018) are particularly relevant to the  
364 current ECS of the Usumacinta–Grijalva Delta on the Gulf of Mexico, which was initiated  
365 approximately 1,000 years ago (Fig. 1, Table 2). These authors reconstructed sea surface  
366 temperatures and salinity in the Gulf of Mexico over the past 1,000 years. Their results showed a  
367 marked centennial scale occurrence of sea surface temperature and salinity variations, which  
368 they correlated to widespread precipitation anomalies on adjacent continents.

369         Wave-dominated deltas with relatively small drainage basins (Table 2), and single  
370 distributary channels located in the same position at the coastline for thousands of years (Figs. 1,  
371 10, 11) would be extremely sensitive to precipitation variations in their catchments; i.e., the





422 in cross-section. As such, when draped by shales, these clinofolds have the potential to impact  
423 fluid flow in reservoirs. Element-complex set and element-set clinofolds are likely to be the  
424 most extensive surfaces and hence the most critically important surfaces for influencing fluid  
425 flow in reservoirs.

426 5) The centennial-scale recurrence of high and low F/W element-set pairs observed near long-  
427 lived (1,000 to 2,500 years), Holocene, wave-dominated delta river-mouths are suggestive of an  
428 external forcing mechanism to drive the cyclicity.

429 6) It is proposed that centennial-scale climate cycles may well provide an external control on the  
430 internal morphology of wave-dominated deltas. Therefore, observations of beach-ridge element-  
431 set and element-set-pair morphology on ancient deltas may be used as a potential proxy for  
432 centennial-scale climate forcing in deep geological time. However, further work is required on  
433 detailed dating of beach-ridge sets on more modern wave-dominated deltas to expand the dataset  
434 available for substantiating this hypothesis.

#### 435 ACKNOWLEDGMENTS

436 Many thoughts and concepts used in this paper were initially developed as a result of  
437 work conducted with funding provided to the *WAVE* Consortium at the Australian School of  
438 Petroleum, University of Adelaide (RBA, BKV and JB). The consortium sponsors (Apache,  
439 BAPETCO, BHPBP, BG, BP, Chevron, ConocoPhillips, Nexen, OMV, Shell, Statoil, Todd  
440 Energy, and Woodside Energy) are thus thanked for making this work possible. We are indebted  
441 to journal reviewers Cornel Olariu and Howard Feldman, and to Associate Editor Janok  
442 Bhattacharya for numerous comments and suggestions that improved the clarity of the  
443 manuscript.

#### 444 REFERENCES

- 445 AINSWORTH, R.B. 1994, Marginal marine sedimentology and high-resolution sequence analysis:  
446 Bearpaw - Horseshoe Canyon transition, Drumheller, Alberta: Bulletin of Canadian  
447 Petroleum Geology, v. 42, p. 26-54.
- 448 AINSWORTH, R.B., SANLUNG, M., AND DUIVENVOORDEN, S.T.C., 1999, Correlation techniques,  
449 perforation strategies, and recovery factors: An integrated 3-D reservoir modeling study,  
450 Sirikit field, Thailand: American Association of Petroleum Geologists, Bulletin, v. 83, p.  
451 1535–1551.
- 452 AINSWORTH, R.B., VAKARELOV, B.K., AND NANSON, R.A., 2011, Dynamic spatial and temporal  
453 prediction of changes in depositional processes on clastic shorelines: Toward improved  
454 subsurface uncertainty reduction and management: American Association of Petroleum  
455 Geologists, Bulletin, v. 95, p. 267-297.
- 456 AINSWORTH, R.B., VAKARELOV, B.K., LEE, C., MACEACHERN, J.A., MONTGOMERY, A.E., RICCI,  
457 L.P., AND DASHTGARD, S.E., 2015, Architecture and evolution of a regressive, tide-  
458 influenced marginal marine succession, Drumheller, Alberta, Canada: Journal of  
459 Sedimentary Research, v. 85, p. 596-625, [dx.doi.org/10.2110/jsr.2015.33](http://dx.doi.org/10.2110/jsr.2015.33).
- 460 AINSWORTH, R.B., VAKARELOV, B.K., MACEACHERN, J.A., NANSON, R.A., LANE, T.I., RARITY, F.  
461 AND DASHTGARD, S.E., 2016. Process-Driven Architectural Variability in Mouth-Bar  
462 Deposits: A Case Study from a Mixed-Process Mouth-Bar Complex, Drumheller, Alberta,  
463 Canada: Journal of Sedimentary Research, v. 86, p. 512-541. DOI:  
464 <http://dx.doi.org/10.2110/jsr.2016:23>
- 465 AINSWORTH, R.B., VAKARELOV, B.K., MACEACHERN, J.A., RARITY, F., LANE, T.I., AND NANSON,  
466 R.A., 2017, Anatomy of a shoreline regression: implications for the high-resolution  
467 stratigraphic architecture of deltas: Journal of Sedimentary Research, v. 87, p. 425-459, doi:  
468 <http://dx.doi.org/10.2110/jsr.2017.26>

- 469 AINSWORTH, R.B., MCARTHUR, J.B. LANG, S.C., AND VONK, A.J., 2018. Quantitative sequence  
470 stratigraphy: AAPG Bulletin, v. 102, p. 1913-1939. doi:10.1306/02201817271
- 471 BHATTACHARYA, J.P., AND WALKER, R.G., 1992, Facies and facies successions in river- and  
472 wave-dominated depositional systems of the Upper Cretaceous Dunvegan Formation,  
473 northwestern Alberta: Bulletin of Canadian Petroleum Geology, v. 39, p. 165-191.
- 474 BHATTACHARYA, J.P., AND GIOSAN, L., 2003, Wave-influenced deltas: geomorphological  
475 implications for facies reconstruction: Sedimentology, v. 50, p. 187-210.
- 476 CHARVIN, K., HAMPSON, G. J., GALLAGHER, K. L., AND LABOURDETTE, R., 2010, Intra-  
477 parasequence architecture of an interpreted asymmetrical wave-dominated delta:  
478 Sedimentology, v. 57, p. 760–785.
- 479 CHARVIN, K., HAMPSON, G.J., GALLAGHER, K.L., STORMS, J.E.A., AND LABOURDETTE, R., 2011,  
480 Characterization of controls on high-resolution stratigraphic architecture in wave-dominated  
481 shoreface–shelf parasequences using inverse numerical modelling: Journal of Sedimentary  
482 Research, v. 81, p. 562–578.
- 483 DOMINGUEZ, J.M.L., BITTENCOURT, A.C.S.P., AND MARTIN, L.M., 1983, O papel da deriva  
484 litoranea de sedimentos arenosos na construcao das planicies costeiras associadas as  
485 desembocaduras dos rios Sao Francisco (SE-AL), Jequitinhonha (BA), Doce (ES), e Paraiba  
486 do Sul (RJ): Revista Brasileira de Geociencias, v. 13, p. 98-105.
- 487 DOMINGUEZ, J.M.L., MARTIN, L.M., AND BITTENCOURT, A.C.S.P., 1987, Sea-level and  
488 quaternary evolution of river mouth-associated beach ridge plains along the east-southeast  
489 Brazilian Coast: A summary, in Nummedal, D., Pilkey, O.H., and Howard, J.D., eds., Sea-  
490 level Fluctuation and Coastal Evolution: SEPM, Special Publication 41, p. 115-127.
- 491 EIDE, C.H., HOWELL, J.A., AND BUCKLEY, S., 2014, Distribution of discontinuous mudstone beds  
492 within wave-dominated shallow-marine deposits: Star Point Sandstone and Blackhawk  
493 Formation, Eastern Utah: AAPG Bulletin, v. 98, p. 1401-1429.



- 494 EIDE, C.H., HOWELL, J.A. AND BUCKLEY, S.J., 2015, Sedimentology and reservoir properties of  
 495 tabular and erosive offshore transition deposits in wave-dominated, shallow-marine strata:  
 496 Book Cliffs, USA. *Petroleum Geoscience* v. 21, p. 55-73.
- 497 FAWCETT, P. J., WERNE, J.P., ANDERSON. R.S., HEIKOOP, J.M., BROWN, E.T, BERKE, M.A.,  
 498 SMITH, S.J., GOFF, F., DONOHOO-HURLEY, L., CISNEROS-DOZAL, L.M., SCHOUTEN, S.,  
 499 SINNINGHE DAMSTE, J.S., HUANG, Y., TONEY, J., FESSENDEN, J., WOLDEGABRIEL, G.,  
 500 ATUDOREI, V., GEISSMAN J.W. AND ALLEN, C. D., 2011, Extended megadroughts in the  
 501 southwestern United States during Pleistocene interglacials: *Nature*, v. 470 (7335), p. 518–  
 502 521.
- 503 FRAZIER, D.E., 1967, Recent deltaic deposits of the Mississippi River: Their development and  
 504 chronology: *Gulf Coast Association of Geological Societies, Transactions*, v. XVII, p. 287-  
 505 315.
- 506 GRAHAM, G.H., JACKSON, M.D., AND HAMPSON, G.J., 2015, Three-dimensional modeling of  
 507 clinoforms in shallow-marine reservoirs: Part 2. Impact on fluid flow and hydrocarbon  
 508 recovery in fluvial-dominated deltaic reservoirs: *American Association of Petroleum*  
 509 *Geologists, Bulletin*, v. 99, p. 1049–1080, doi: 10.1306/01191513191.
- 510 HAMPSON, G.J., 2000, Discontinuity surfaces, clinoforms, and facies architecture in a wave-  
 511 dominated shoreface-shelf parasequence: *Journal of Sedimentary Research*, v. 70, p. 325-  
 512 340.
- 513 HAMPSON, G.J., AND STORMS, J.E.A., 2003, Geomorphological and sequence stratigraphic  
 514 variability in wave-dominated, shoreface–shelf parasequences: *Sedimentology*, v. 50, p.  
 515 667–701.
- 516 HAMPSON, G.J. AND HOWELL, J.A., 2005, Sedimentologic and geomorphic characterization of  
 517 ancient wave-dominated deltaic shorelines: examples from the Late Cretaceous Blackhawk

- 518 Formation, Book Cliffs, Utah, in Bhattacharya, J.P. and Giosan, L., eds., *River Deltas:*  
 519 *Concepts, Models, and Examples*: SEPM, Special Publication 83, p. 133–154.
- 520 HAMPSON, G.J., RODRIGUEZ, A.B., STORMS, J.E.A., JOHNSON, H.D., AND MEYER, C.T., 2008,  
 521 Geomorphology and high-resolution stratigraphy of progradational wave-dominated  
 522 shoreline deposits: Impact on reservoir-scale facies architecture, *in* Hampson, G.J., Steel,  
 523 R.J., Burgess, P.M. and Dalrymple, R.W., eds., *Recent Advances in Models of Siliciclastic*  
 524 *Shallow-Marine Stratigraphy*: SEPM, Special Publication 90, p. 117–142.
- 525 HIGGS, K.E, KING, P.R., RAINE, J.I., SYKES, R., BROWNE, G.H., CROUCH, E.M., BAUR, J.R., 2012,  
 526 Sequence stratigraphy and controls on reservoir sandstone distribution in an Eocene  
 527 marginal marine-coastal plain fairway, Taranaki Basin, New Zealand: *Marine and Petroleum*  
 528 *Geology*, v. 32, p. 110-137.
- 529 JACKSON, C.A.L., GRUNHAGEN, H., HOWELL, J.A., LARSEN, A.L., ANDERSSON, A, BOEN, F., AND  
 530 GROTH, A., 2010, 3D seismic imaging of lower delta-plain beach ridges: lower Brent Group,  
 531 northern North Sea: *Journal of the Geological Society, London*, v. 167, p. 1225–1236. doi:  
 532 10.1144/0016-76492010-053.
- 533 KARNAUSKAS, K.B., SMERDON, J.E., SEAGER, R., AND GONZALEZ-ROUCO, J.F., 2012, A Pacific  
 534 centennial oscillation predicted by coupled GCMs: *Journal of Climate*, v. 25, p. 5943-5961.  
 535 DOI: 10.1175/JCLI-D-11-00421.1.
- 536 LANE, T. I., 2016. Evolution and Architecture of the Holocene Mitchell River Megafan and Delta,  
 537 Gulf of Carpentaria, Australia: Ph.D. dissertation, University of Adelaide, Adelaide,  
 538 Australia, 718 p. <http://hdl.handle.net/2440/112590>
- 539 LANE, T. I., NANSON, R. A., VAKARELOV, B. K., AINSWORTH, R. B., DASHTGARD, S.S., 2017,  
 540 Evolution and architectural styles of a forced-regressive Holocene delta and megafan,  
 541 Mitchell River, Gulf of Carpentaria, Australia, *in*, Hampson, G.J., Reynolds, A.D., Kostic,  
 542 B., and Wells, M.R., eds., *Sedimentology of Paralic Reservoirs: Recent Advances*,

- 543 Geological Society, London, Special Publication 444, p. 305-334.  
 544 <http://doi.org/10.1144/SP444.9>
- 545 LODICO, J.M., FLOWER, B.P., AND QUINN, T.M., 2006, Subcentennial-scale climatic and  
 546 hydrologic variability in the Gulf of Mexico during the early Holocene: *Paleoceanography*,  
 547 v. 21, PA3015, doi:10.1029/2005PA001243.
- 548 MARTIN, L.M., DOMINGUEZ, J.M.L., AND BITTENCOURT, A.C.S.P., 1985, Roundness in Holocene  
 549 sands of the Paraiba do Sul coastal plain, Rio de Janeiro, Brazil: *Journal of Coastal*  
 550 *Research*, v. 1, p. 343-351.
- 551 MARTIN, L., SUGUIO, K., AND FLEXOR, J.M., 1993, As flutuações de nível do mar durante o  
 552 Quaternário superior e a evolução geológica de “deltas” brasileiros: *Boletim IG/ USP*, 15, 1-  
 553 186.
- 554 MARTIN, L.M., DOMINGUEZ, J.M.L., AND BITTENCOURT, A.C.S.P., 2003, Fluctuating Holocene  
 555 Sea Levels in Eastern and Southeastern Brazil: Evidence from Multiple Fossil and  
 556 Geometric Indicators: *Journal of Coastal Research*, v. 19, p. 101-124.
- 557 MIALL, A., 2015, Updating uniformitarianism: Stratigraphy as just a set of ‘frozen accidents’, *in*  
 558 Smith, D.G., Bailey, R.J., Burgess, P.M., and Fraser, A.J., eds., *Strata and Time: Probing the*  
 559 *Gaps in Our Understanding*: Geological Society of London, Special Publication 404, p. 11–  
 560 36. <http://dx.doi.org/10.1144/SP404.4>
- 561 MITCHUM, R.M. Jr., and J.C. VAN WAGONER, 1991, High-frequency sequences and their  
 562 stacking patterns: sequence-stratigraphic evidence of high-frequency eustatic cycles:  
 563 *Sedimentary Geology*, v. 70, p. 131-160.
- 564 NANSON, R.A., VAKARELOV, B.K., AINSWORTH, R.B., WILLIAMS, F.M., AND PRICE, D.M., 2013,  
 565 Evolution of a Holocene, mixed-process, forced regressive shoreline: The Mitchell river  
 566 delta, Queensland, Australia: *Marine Geology*, v. 339, p. 22-43.

- 567 NEWBY, P.E., SHUMAN, B.N., DONNELLY, J.P., KARNAUSKAS, K.B., AND MARSICEK, J., 2014,  
 568 Centennial-to-millennial hydrologic trends and variability along the North Atlantic Coast,  
 569 USA, during the Holocene: *Geophysical Research Letters*, v. 41, p. 4300–4307,  
 570 doi:10.1002/ 2014GL060183.
- 571 NOOREN, K., HOEK, W.Z., WINKELS, T., HUIZINGA, A, VAN DER PLICHT, H., VAN DAM, R.L., VAN  
 572 HETEREN, S., VAN BERGEN, M.J., PRINS, M.A., REIMANN, T., WALLINGA, J., COHEN, K.M.,  
 573 MINDERHOUD, P., AND MIDDELKOOP, H., 2017, The Usumacinta–Grijalva beach-ridge plain  
 574 in southern Mexico: a high-resolution archive of river discharge and precipitation: *Earth  
 575 Surface Dynamics*, v. 5, p. 529-556.
- 576 OTVOS, E.G., 2000, Beach ridges - definitions and significance: *Geomorphology*, v. 32, p. 83-  
 577 108.
- 578 PATTISON, S.A.J., 1995, Sequence stratigraphic significance of sharp-based lowstand shoreface  
 579 deposits, Kenilworth Member, Book Cliffs, Utah: *American Association of Petroleum  
 580 Geologists Bulletin*, v. 79, p. 444-462.
- 581 RODRIGUEZ, A.B., HAMILTON, M.D., AND ANDERSONN, J.B., 2000, Facies and evolution of the  
 582 modern Brazos Delta, Texas: Wave versus flood influence: *Journal of Sedimentary  
 583 Research*, v. 70, p. 283-295.
- 584 SANCHEZ C.M., FULTHORPE, C.S., AND STEEL, R.J., 2012, Middle Miocene–Pliocene siliciclastic  
 585 influx across a carbonate shelf and influence of deltaic sedimentation on shelf construction,  
 586 Northern Carnarvon Basin, Northwest Shelf of Australia: *Basin Research*, v. 24, p. 664-682,  
 587 DOI: 10.1111/j.1365-2117.2012.00546.x
- 588 SANJAUME, E., AND TOLGENSBAKK, J., 2009, Beach ridges from the Varanger Peninsula (Arctic  
 589 Norwegian coast): Characteristics and significance: *Geomorphology*, v. 104, p. 82-92.
- 590 SECH, R. P., JACKSON, M. D., AND HAMPSON, G. J., 2009, Three-dimensional modeling of a  
 591 shoreface-shelf parasequence reservoir analog: Part 1. Surface-based modeling to capture

- 592 high resolution facies architecture: American Association of Petroleum Geologists, Bulletin,  
593 v. 93, p. 1155–1181, doi:10.1306/05110908144.
- 594 SØMME, T.O., HOWELL, J.A., AND HAMPSON, G.J., AND STORMS, J.E.A., 2008, Genesis,  
595 architecture, and numerical modeling of intra-parasequence discontinuity surfaces in wave-  
596 dominated deltaic deposits: Upper Cretaceous Sunnyside Member, Blackhawk Formation,  
597 Book Cliffs, Utah, U.S.A., in Hampson, G.J., Steel, R.J., Burgess, P.M., and Dalrymple,  
598 R.W., eds., Recent Advances in Models of Shallow-Marine Stratigraphy: SEPM, Special  
599 Publication 90, p. 421-441.
- 600 STORMS, J.E.A., AND HAMPSON, G.J., 2005, Mechanisms for forming discontinuity surfaces  
601 within shoreface-shelf parasequences: Sea level, sediment supply or wave regime?: Journal  
602 of Sedimentary Research, v. 75, p. 67–81, doi: 10.2110/jsr.2005.007.
- 603 TAMURA, T., 2012, Beach ridges and prograded beach deposits as palaeoenvironment records:  
604 Earth-Science Reviews, v. 114, p.279-297.
- 605 TAYLOR, D.R., and LOVELL, R.W.W., 1995, High-frequency sequence stratigraphy and  
606 paleogeography of the Kenilworth Member, Blackhawk Formation, Book Cliffs, Utah,  
607 U.S.A., in Van Wagoner, J.C. and Bertram, G.T., eds., Sequence Stratigraphy of Foreland  
608 Basin Deposits: American Association of Petroleum Geologists, Memoir 64, p. 257-275.
- 609 THIRUMALAI, K., QUINN, T.M., OKUMURA, Y., RICHEY, J.N., PARTIN, J.W., POORE, R.Z., AND  
610 MORENO-CHAMARRO, E., 2018, Pronounced centennial-scale Atlantic Ocean climate  
611 variability correlated with Western Hemisphere hydroclimate: Nature Communications  
612 (2018) 9392, DOI: 10.1038/s41467-018-02846-4.
- 613 VAKARELOV, B.K., AND AINSWORTH, R.B., 2013, A hierarchical approach to architectural  
614 classification in marginal marine systems – bridging the gap between sedimentology and  
615 sequence stratigraphy: American Association of Petroleum Geologists Bulletin, v. 97, p.  
616 1121-1161.

617 VAN SAPAROEVA, A.P.H.V.D.B., AND POSTMA, G., 2008, Control of climate change on the yield of  
 618 river systems, in Hampson, G.J., Steel, R.J., Burgess, P.M., and Dalrymple, R.W., eds.,  
 619 Recent Advances in Models of Shallow-Marine Stratigraphy: SEPM, Special Publication 90,  
 620 p. 15-33.

621 VAN WAGONER, J.C., 1995, Sequence stratigraphy and marine to nonmarine facies architecture  
 622 of foreland basin strata, Book Cliffs, Utah, U.S.A., in Van Wagoner, J.C., and Bertram,  
 623 G.T., eds., Sequence Stratigraphy of Foreland Basin Deposits: American Association of  
 624 Petroleum Geologists, Memoir 64, p. 137-223.

625 VASCONCELOS, S.C., ABUCHACRA, R.C., ROCHA, T.B. AND FERNANDEZ, G.B., 2016, Análise  
 626 comparativa dos padrões morfoestratigráficos em deltas assimétricos, exemplo do delta do  
 627 Rio Paraíba do Sul (RJ): XI SINAGEO - Simpósio Nacional de Geomorfologia - UGB -  
 628 União da Geomorfologia Brasileira, 7 p.

629 <http://www.sinageo.org.br/2016/trabalhos/7/76061739.html>

630

### 631 **FIGURE CAPTIONS**

632 **FIG. 1.** A) Location map for the Usumacinta–Grijalva Delta, Mexico. B) Location map for the  
 633 current symmetrical delta lobe (element complex set; ECS). C) Detailed stratigraphic  
 634 architecture depicting beach-ridge elements and beach-ridge sets (element sets; ES). Note the  
 635 mouth-bar ES units (high F/W) combine with the lobe ES units (low F/W) to form ES pairs. D)  
 636 Inset map showing detail of element-set pairs. E) Bathymetric contours of the current mouth-bar  
 637 area interpreted from data supplied by Navionics  
 638 (<https://www.navionics.com/aus/apps/navionics-boating>). An element complex (EC) is the  
 639 equivalent of a facies association (Table 1; Vakarelov and Ainsworth, 2013). Base maps from  
 640 Google Earth. Interpretation from *WAVE* Knowledgebase 3 (<https://sedbase.com>).

641 **FIG. 2.** Symmetrical wave-dominated delta architectural summary. A) High order architectural  
 642 units; elements, element sets and element-set pairs. B) Intermediate order architectural units.  
 643 Groupings of lower order units into element complexes (similar to facies associations). Mouth  
 644 bar and lobe element-complexes illustrated. C) Sedimentary log cross-section illustrating vertical  
 645 expression of architectural units shown in plan views in parts A) and B). See Table 1, the text  
 646 and Vakarelov and Ainsworth (2013) for more detailed explanations and definitions of  
 647 architectural units.

648 **FIG. 3.** Vertical section through a Holocene wave-dominated mouth-bar. See location maps at  
 649 top right for the Mitchell River Delta system, Gulf of Carpentaria, Queensland, NE Australia.  
 650 The core sedimentary log and depositional environmental interpretation is from Lane (2016).  
 651 Note the Holocene wave-dominated, fluvial-influenced, tide-affected (Wft) mouth-bar deposits  
 652 exhibit the element (bedset), element-set and element-complex-set architecture depicted in the  
 653 schematic in Fig. 2C. Compare with the similar stratigraphic architectures shown in the ancient  
 654 examples in Figs. 5-8. The recognition of key surfaces such as the ECS boundary at 6.5 m is  
 655 cryptic when using only core sedimentary log data alone. The stacking pattern rules of elements  
 656 (bedsets) and element sets are critical for picking these key surfaces (Ainsworth et al. 2017).  
 657 Also note that in this low accommodation system (5.5 m water depth), the preservation potential  
 658 of the capping 2.5 m of eolian deposits is relatively low since they are likely to be removed  
 659 during the next transgressive wave ravinement event. The two age dates are from optically  
 660 stimulated luminescence (OSL) analyses; see Lane (2016) for details. Base maps from Google  
 661 Earth. Interpretation from *WAVE* Knowledgebase 3 (<https://sedbase.com>).

662 **FIG. 4.** A) Random seismic line cross section in two-way time (TWT) across the Bare  
 663 Formation, Northwest Shelf, Australia (Middle Miocene to Pliocene). Location of seismic line  
 664 X-Y shown on map (B). B) Route mean square (RMS) amplitude attribute map of seismic  
 665 horizon in (A). Red and orange colors correspond to higher RMS amplitudes, white colors to

666 lower RMS amplitudes. The map shows a north to north-north-west prograding wave-dominated  
 667 delta fed by small fluvial systems (F). Wide areas of higher RMS amplitudes are interpreted as  
 668 lagoon or lake settings (L) where dolomites, dolomitized sandstones and calcarenites have  
 669 accumulated (Sanchez et al. 2012). Areas associated in map view with linear, sub-parallel  
 670 geometries are interpreted as beach ridges (BR). C) Rio Coco partial analog from the Honduras  
 671 and Guatemala border region. Interpretation from WAVE Knowledgebase 3  
 672 (<https://sedbase.com>). D) and E) Inset map (see part B) of RGB-color blending of spectral  
 673 decomposition frequency attributes at 13, 36 and 57 Hertz. Compare the stratigraphic  
 674 architectures with those observed on the Holocene delta in Figure 1 and summary Figure 2.

675 **FIG. 5.** Wave-dominated delta, Mangahewa Formation, Eocene, New Zealand. An example of  
 676 ancient beach-ridges shown in plan-view (right) on a 3D seismic-attribute map (minimum  
 677 acoustic impedance, 10 millisecond time window). The low impedance events (gray colors) in  
 678 the south-east of the area are present day coals, which would be related to swamp conditions at  
 679 the time of deposition. The contrast between the low impedance coals in the beach-ridge swales  
 680 with the beach ridges themselves enables visualization of the beach ridge geometries. The  
 681 equivalent interval of the seismic attribute map is shown for two wells, one with core (POS-01)  
 682 and one with gamma ray (GR) wireline data (POS-01B). Note the stratigraphic architecture at  
 683 element, element-set and element-complex-set scales, described in Fig. 2C, is also recognizable  
 684 in these deposits. ts = transgressive surface; tse = transgressive surface of erosion; mfs =  
 685 maximum flooding surface. All surfaces are fifth order ( $10^4$  to  $10^5$  years; Ainsworth et al. 2018).

686 **FIG. 6.** Outcrop lidar photo panel showing a depositional strike section of the wave-dominated  
 687 delta-lobe deposits of the Sunnyside Member of the Blackhawk Formation, Utah, USA (Sømme  
 688 et al. 2008). These strata are exposed on the west side of the Beckwith Plateau, 15 km NW of the  
 689 town of Green River (UTM coordinates; 12S 564092 4327978). S2 = Sunnyside parasequence 2  
 690 and S3 = Sunnyside parasequence 3. S2.5, S2.6, S3.1 and S3.2 are previously interpreted intra-



691 parasequence “bedsets” (Sømme et al. 2008; Table 1). These stratigraphic units are the  
692 equivalent of the element complex set (ECS; Figs. 1, 2 and 5). Note that there are two further  
693 levels of hierarchy recognized at a smaller scale, element set (ES) and element (E). Compare  
694 with the measured sedimentological logs and wireline data shown in Figs. 5 and 8.

695 **FIG. 7.** A) Uninterpreted outcrop photo panel of the KSP010 wave-dominated delta  
696 parasequence of the Star Point Sandstone, Wasatch Plateau, USA. B) Interpreted photo panel  
697 showing bed or bedset terminations and downlaps (mouth-bar clinoform terminations) onto  
698 element-set boundaries and onlaps (lobe lateral-onlap onto the older mouth-bars) onto element-  
699 set-pair boundaries respectively. The mouth bar and lobe interpretations are from Eide et al.  
700 (2014). See Fig. 8A for interpreted lidar panel of the same interval and Fig. 8B for a measured  
701 sedimentary log. C) Model of idealized element-set pair transitions (taken from Fig. 2). Compare  
702 with the onlap and downlap geometries observed in the outcrop. Center of the distributary  
703 channel in part B) is at UTM coordinates 12S 487910 4338830.

704 **FIG. 8.** A) Outcrop lidar interpreted panel of the KSP010 wave-dominated delta parasequence of  
705 the Star Point Sandstone, Wasatch Plateau, USA. Note the hummocky morphology shown at top  
706 left which may be representative of beach-ridge deposits. See the photo panel of a portion of the  
707 outcrop around the distributary channel and mouth bar in Fig. 7. B) Sedimentary log from a  
708 location adjacent to the cross-section in A. Note the element, element set and element-complex-  
709 set architecture. A and B are both modified from Eide et al. (2014). C) and D) Depositional  
710 model to reconcile the stratigraphic architecture observed on modern symmetrical wave-  
711 dominated deltas (Fig. 1) and ancient wave-dominated deltas (Figs. 4-8). Stratal units are  
712 identified by simple rules: Element sets (ES) are defined by upward-thickening elements (E;  
713 bedsets). Element complex sets (ECS) are formed by upward-thickening element sets.  
714 Regressive element complex assemblage sets (RECAS; regressive systems tract) are formed by  
715 thickening-upward element complex sets (see part B). Stratal unit boundaries are defined by

716 breaks in these thickening-upward trends. Note that in cross-sectional view the three stratal  
 717 surfaces are represented clinoform geometries (i, ii, iii). The shales draping the ECS boundaries  
 718 (iii) are likely to be the most laterally extensive and have the greatest impact on fluid flow in a  
 719 reservoir. Shales draping element (bedset) boundaries (i) are likely to be numerous but relatively  
 720 restricted in their lateral extent. Note that in C) and D), horizontal and vertical scales are  
 721 indicative and somewhat exaggerated in order to depict the architectural styles and stacking  
 722 patterns.

723 **FIG. 9.** Impact of the ratio of *rate of fluvial sediment supply* to *rate of longshore wave transport*  
 724 (F/W) on symmetrical wave-dominated deltas. A) Formation of mouth-bar element set (ES)  
 725 during high F/W. B) Subsequent formation of the lobe element-set “healing phase” during low  
 726 F/W and hence the element-set pair. C) Repeated ES pairs form the delta lobe (element complex  
 727 set; ECS). D) and E) illustrate the changes in F/W ratio through time at two depositional dip  
 728 locations in part C). Note the out-of-phase deposition of the mouth bar ES and the lobe ES. Also  
 729 note the diachroneity of the element-set-pair boundary unconformity and disconformity  
 730 formation in C). Also note the assumption in D) and E) that the time duration for mouth-bar  
 731 element-set and lobe element-set deposition are equal.

732 **FIG. 10.** A) Location map for the Jequitinhonha delta, Brazil. B) Location map for the current  
 733 symmetrical delta lobe (element complex set; ECS). C) Detailed stratigraphic architecture  
 734 depicting beach-ridge elements, beach-ridge sets (element sets; ES) and element-set pairs. The  
 735 mouth-bar ES units are equivalent to the high F/W phases of the delta. The low F/W phases of  
 736 the delta are represented by the healing phase lobe ES. Note the area to the north of the  
 737 distributary channel where geomorphology is difficult to interpret due to the intermittent  
 738 northerly migration of the distributary channel through this area. D) Bathymetric contours of the  
 739 current mouth-bar area interpreted from data supplied by Navionics  
 740 (<https://www.navionics.com/aus/apps/navionics-boating>). Note that the contours of the mouth-

741 bar on the north and south sides of the river mouth mimic the geometry of the high F/W mouth-  
 742 bar element-sets. An element complex (EC) is the equivalent of a facies association (Table 1;  
 743 Vakarelov and Ainsworth, 2013). Base maps from Google Earth. Interpretation from *WAVE*  
 744 Knowledgebase 3 (<https://sedbase.com>).

745 **FIG. 11.** A) Location map for the Paraiba do Sul Delta, Brazil. B) Location map for the current  
 746 asymmetrical delta lobe (element complex set; ECS). C) Detailed stratigraphic architecture  
 747 depicting beach-ridge elements, beach-ridge sets (element sets; ES) and element-set pairs. Note  
 748 that the mouth-bar element-complex is deflected in a downdrift direction hence on the updrift  
 749 flank, lobe ES units rather than mouth-bar ES units (Figs. 1 and 9) represent the high F/W  
 750 periods. The low F/W lobe ES units on the flanks represent the lobe healing phase and they  
 751 combine with the high F/W lobe ES units to form element-set pairs. D) Bathymetric contours of  
 752 the current mouth-bar area interpreted from data supplied by Navionics  
 753 (<https://www.navionics.com/aus/apps/navionics-boating>). Note that the contours of the mouth-  
 754 bar on the updrift side of the river mouth (right side) mimic the geometry of the updrift high F/W  
 755 lobe element-sets in C). An element complex (EC) is the equivalent of a facies association (Table  
 756 1; Vakarelov and Ainsworth, 2013). The uncertainty in the age of the current ECS is due to  
 757 different age dating techniques (Table 2). Base maps from Google Earth. Interpretation from  
 758 *WAVE* Knowledgebase 3 (<https://sedbase.com>).

## 759 TABLE CAPTIONS

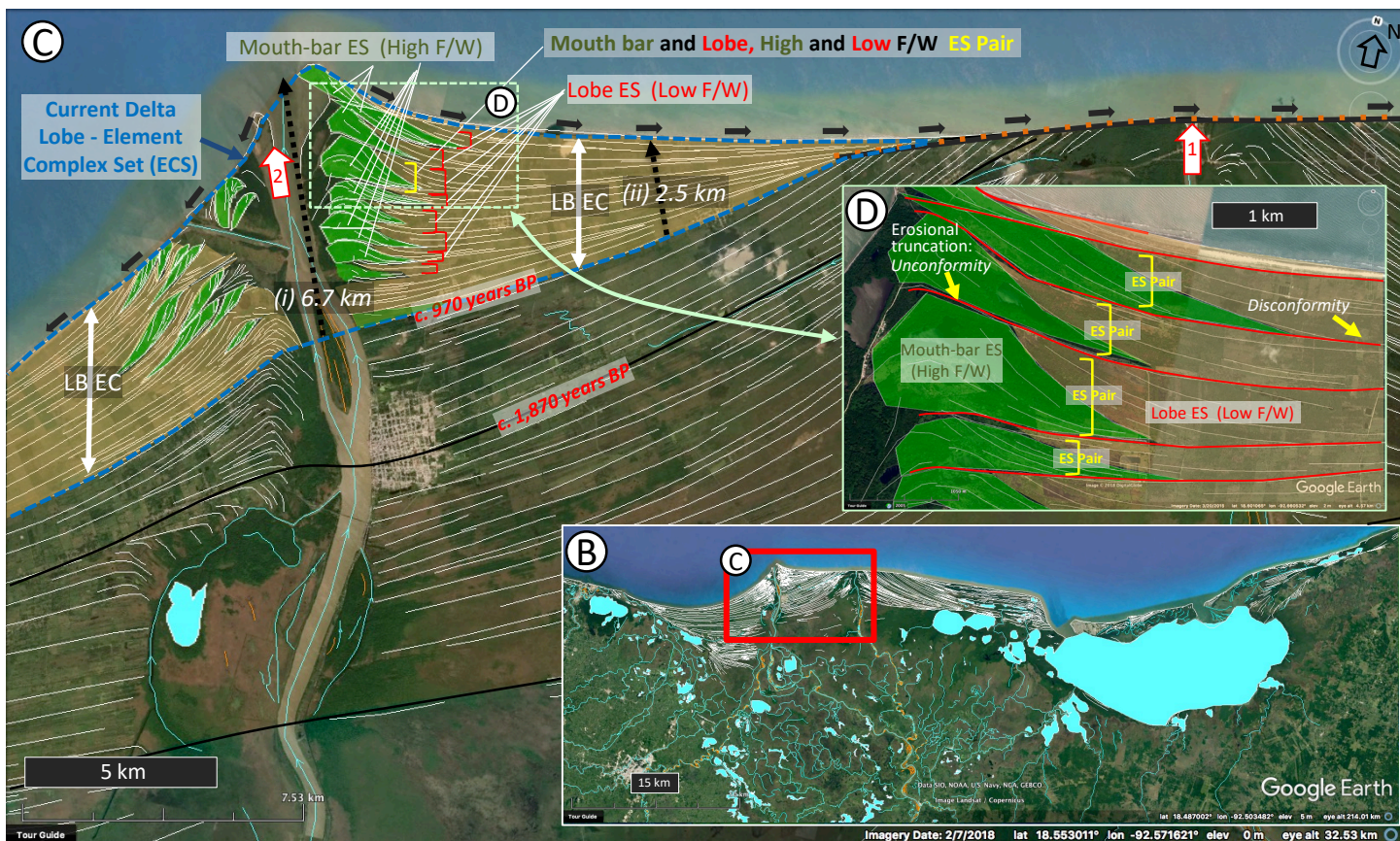
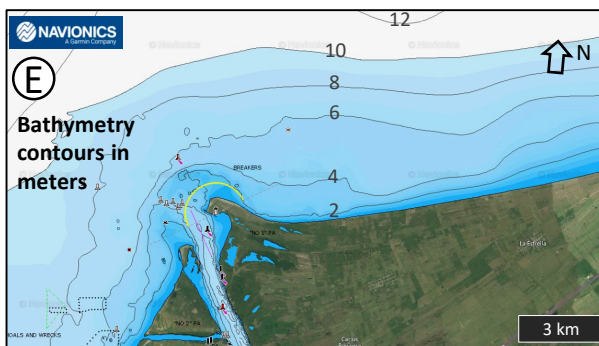
760 **TABLE 1.** Comparison of WAVE Classification terms for both plan and vertical section  
 761 stratigraphic units relevant to wave-dominated deltas (Vakarelov and Ainsworth, 2013;  
 762 Ainsworth et al. 2017) with commonly used geomorphological terms for plan views and  
 763 stratigraphic terms for vertical sections (see Figures 2 and 8). Note that many of the stratigraphic  
 764 units have no common geomorphological term (column 2; NA = not applicable) or vertical  
 765 section stratigraphic term (column 3) making correlation of plan view geometries to vertical

766 section geometries problematical and prone to terminological misunderstandings and errors. Also  
767 note the common and confusing use of the terms “bedset”, “parasequence” and “parasequence  
768 set” at two to three different vertical hierarchical scales (columns 3 and 4). The WAVE  
769 Classification (column 1) provides a consistent and coherent language for comparing plan  
770 section and vertical-section stratigraphic architectures. Abbreviations of WAVE terms are shown  
771 in italics at the end of the descriptions in column 1.

772 **TABLE 2.** Data for three Holocene delta lobes (element complex sets; ECS). Note the duration  
773 of element set (ES) pairs for each delta is estimated at around 100 to 200 years. Data for the  
774 Paraiba do Sul from Martin et al. (1993) and Vasconcelos et al. (2016), the Jequitinhonha delta  
775 from Martin et al. (1993), and the Usumacinta–Grijalva delta from Nooren et al. (2017). <sup>14</sup>C =  
776 Carbon 14 absolute dating methods. OSL = optically stimulated luminescence absolute dating  
777 methods. N.B. absolute age durations have an uncertainty associated with the measurements (see  
778 details in relevant sources), hence they are stated as approximate durations (c. = circa).

779 **TABLE 3.** Description, probable timeframe of deposition, response type and formative  
780 mechanism for architectural units on wave-dominated deltas.

# Usumacinta-Grijalva Delta, Mexico



--- Current Element Complex Set (ECS; delta lobe) boundary / Older ECS boundary

--- Unconformity (ECS scale)

--- Unconformity & Disconformity (ES scale)

↕ Major fluvial point source depocenter (delta lobe or element complex set)

▨ Element - Beach ridge

▨ Element set (ES) - Beach ridge set

▨ Centerline of watercourse

MB = Mouth bar LB = Lobe

↕ Element complex (EC)

← Present day dominant longshore transport direction

▨ ES - High F/W

▨ ES - Low F/W

Fig. 1





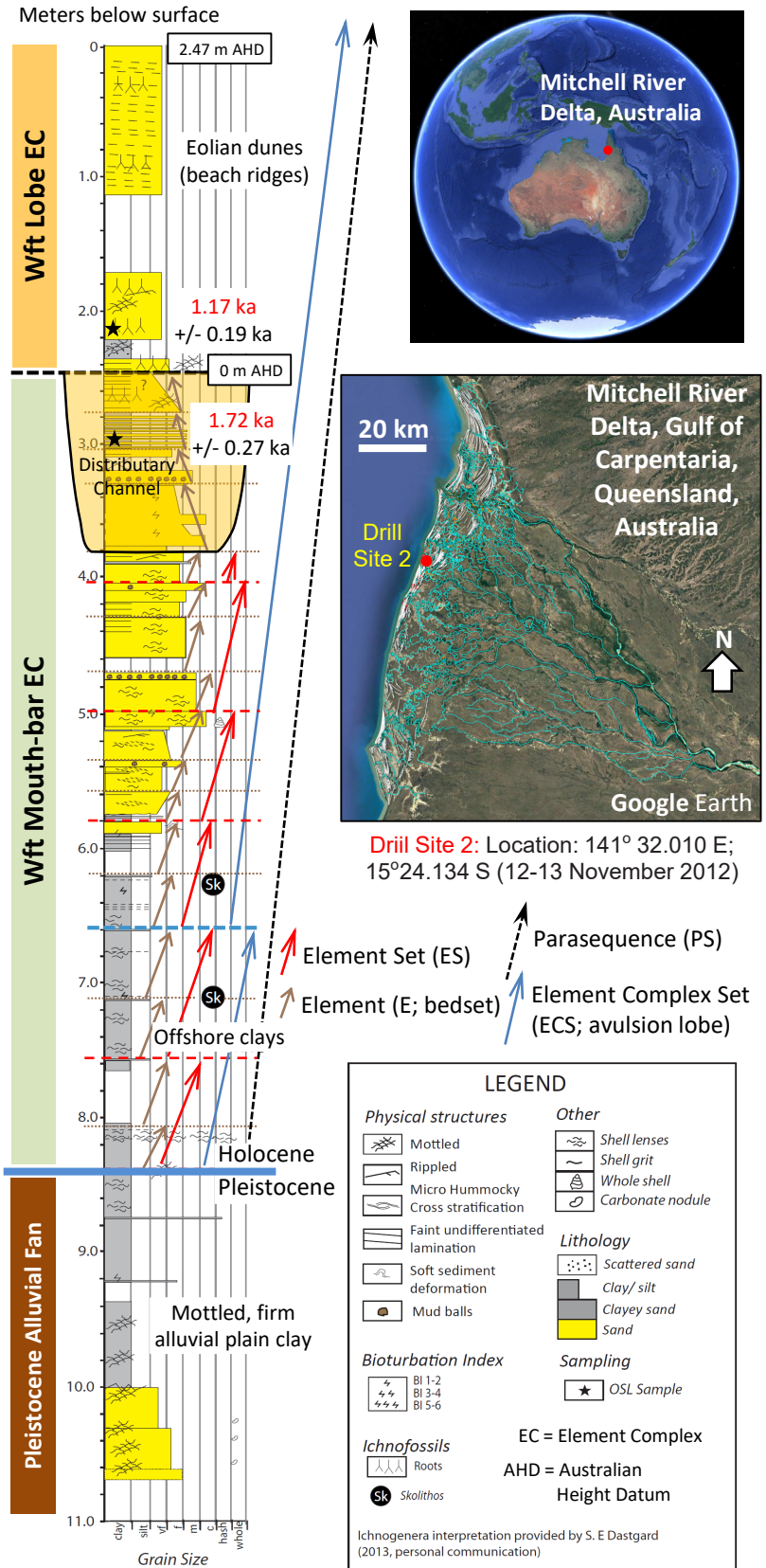


Fig. 3

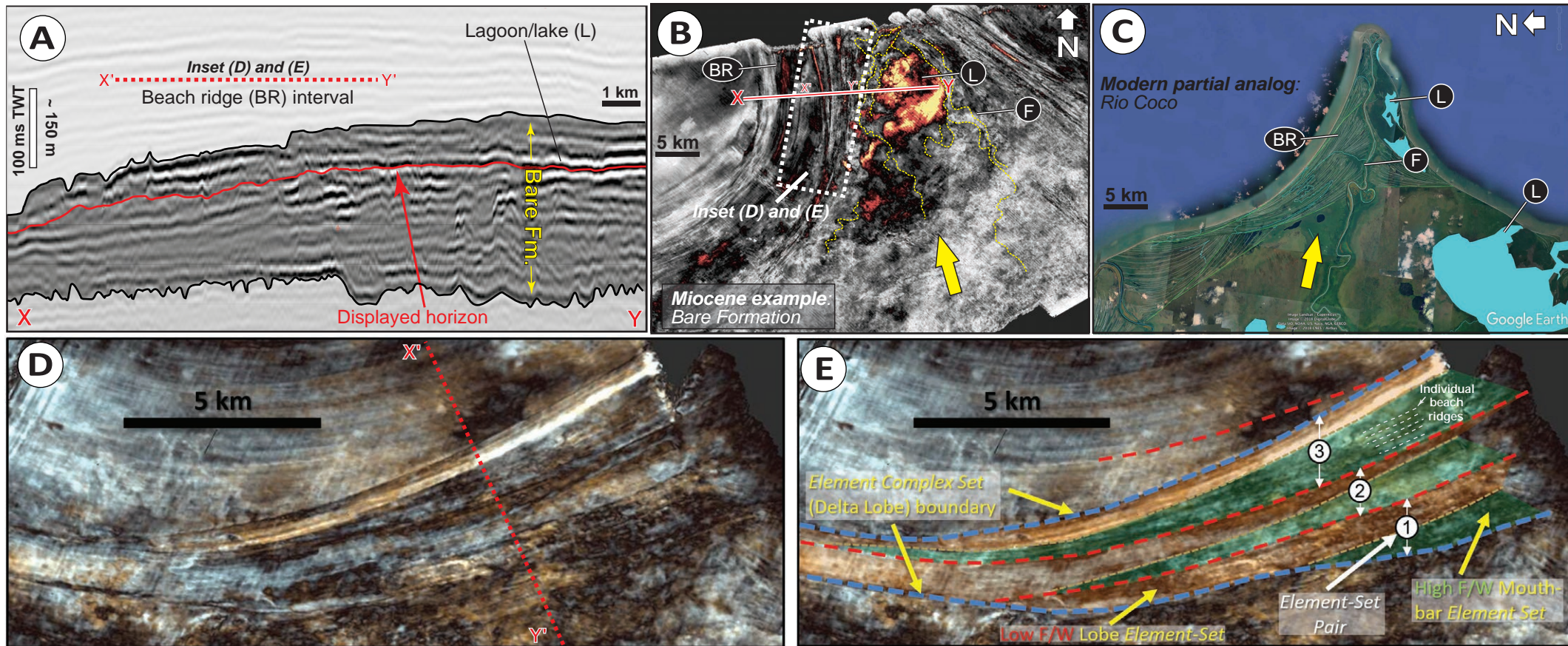


Fig. 4



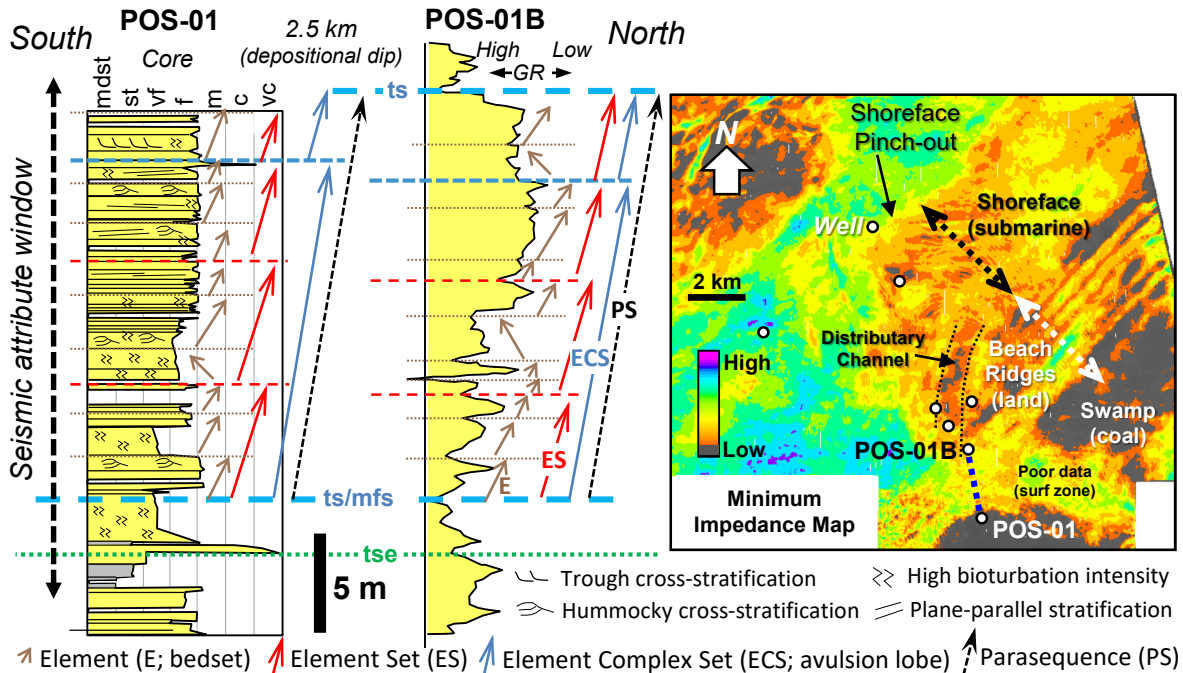


Fig. 5



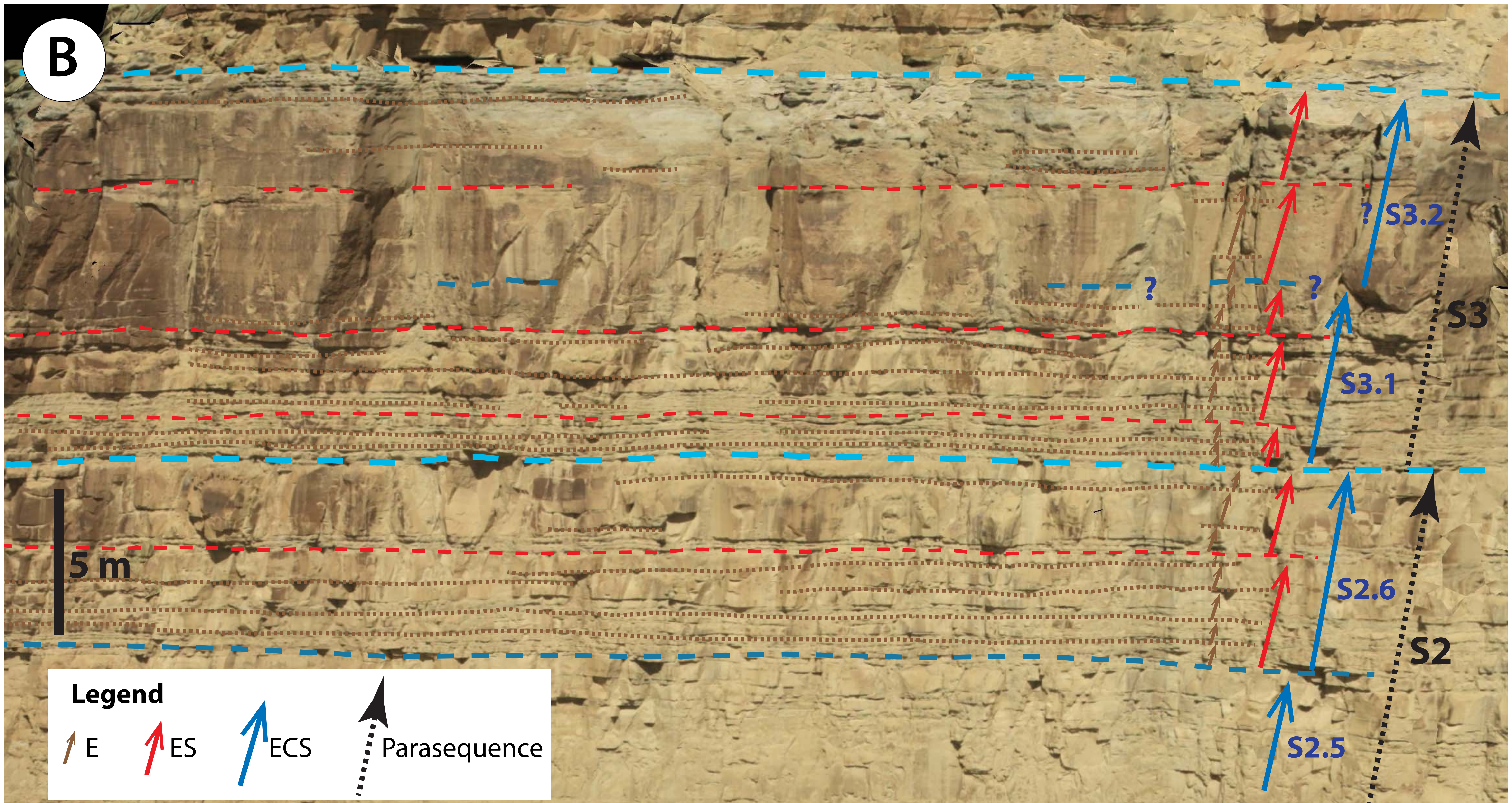
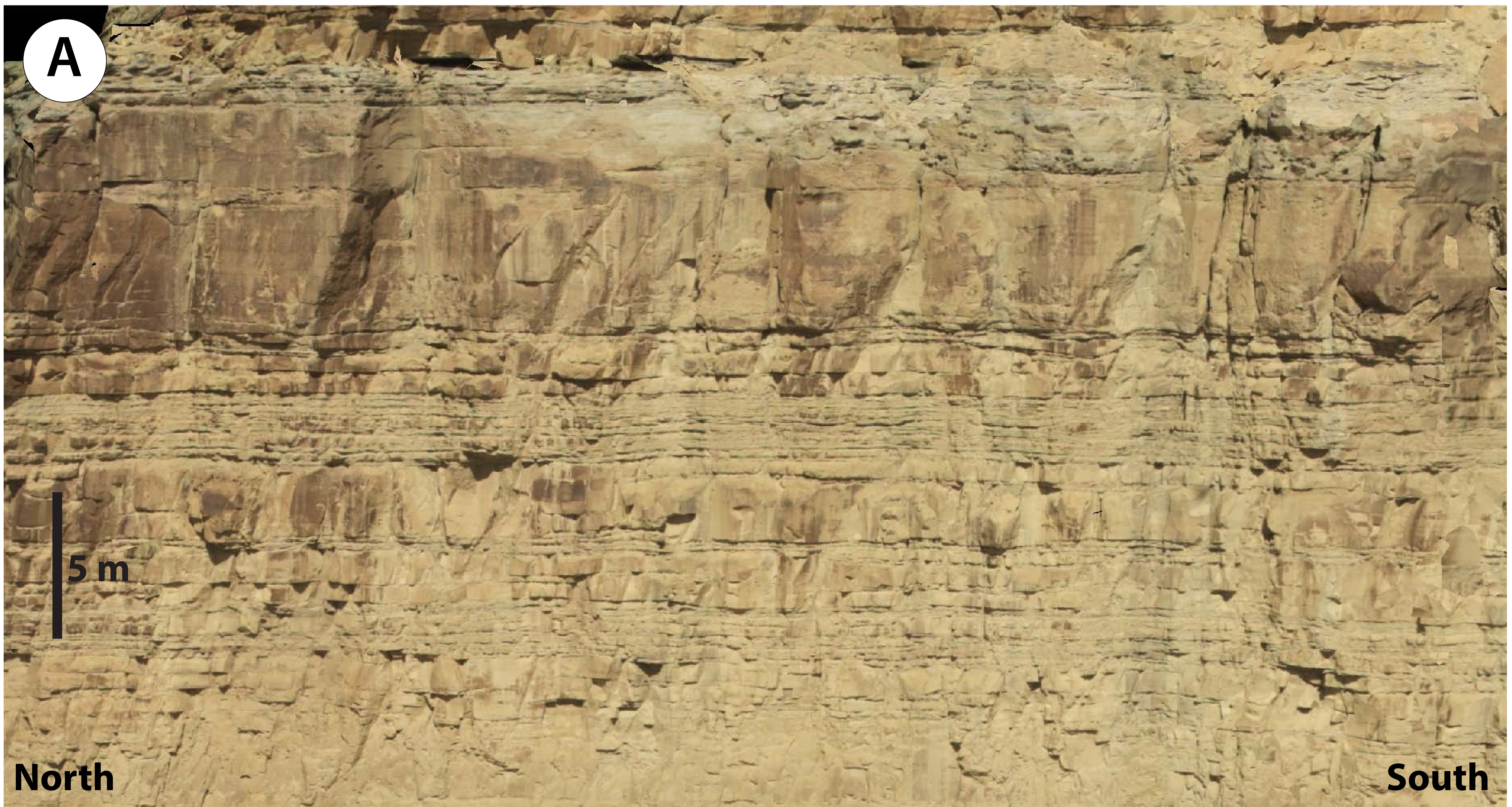
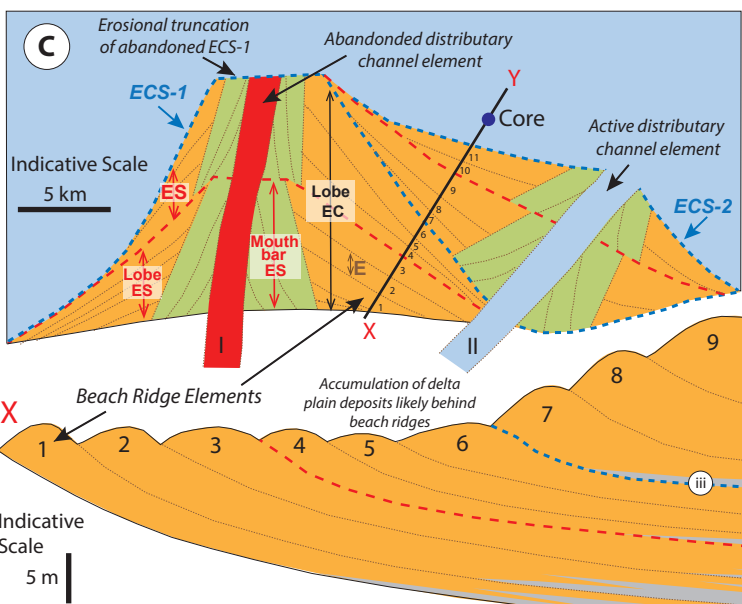
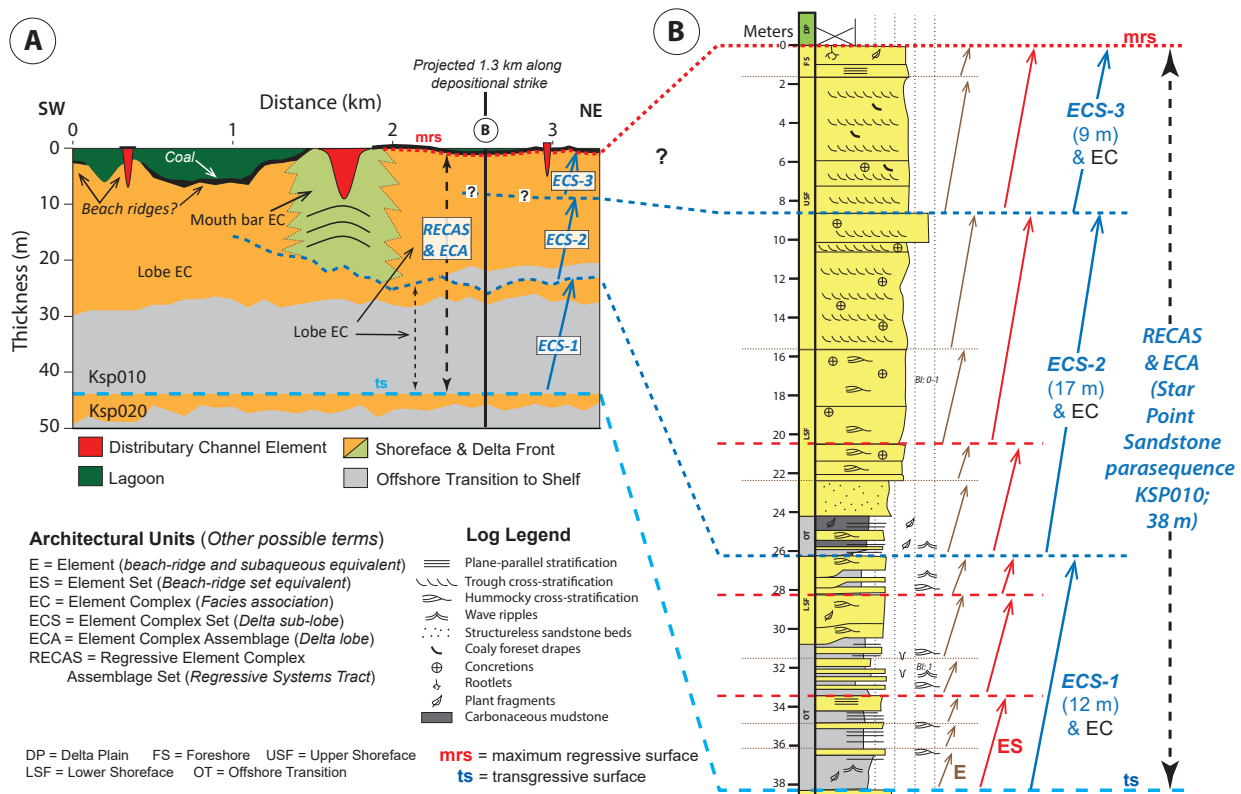


Fig. 6

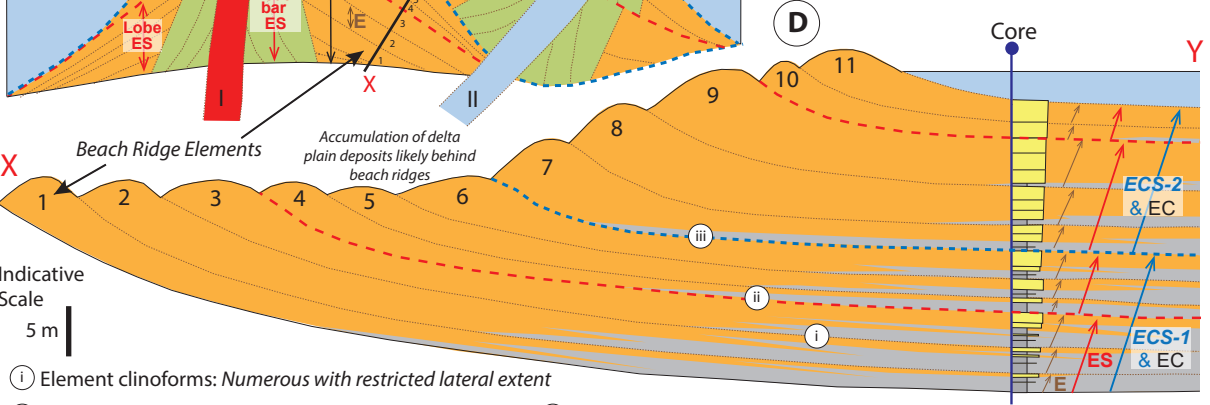






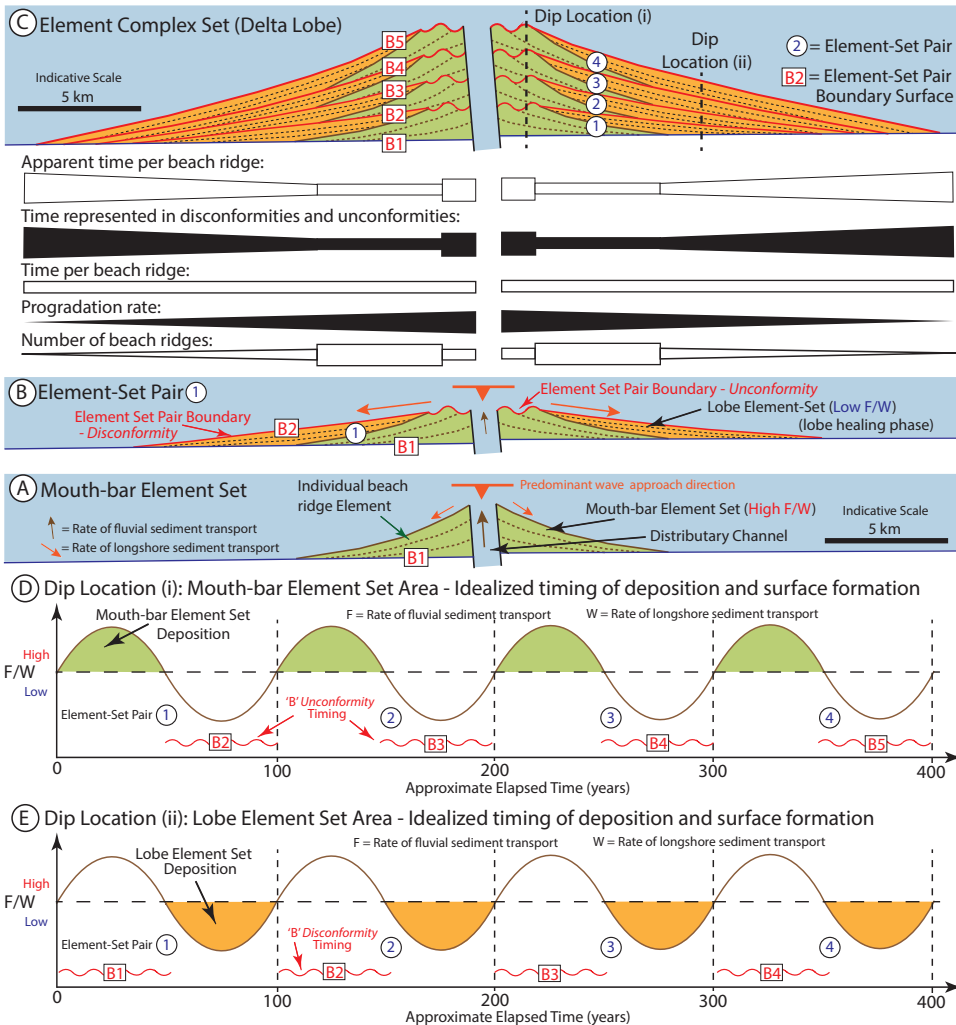


N.B. Both examples illustrate high accommodation shorelines (Ainsworth et al. 2017) with climbing shoreline trajectories.

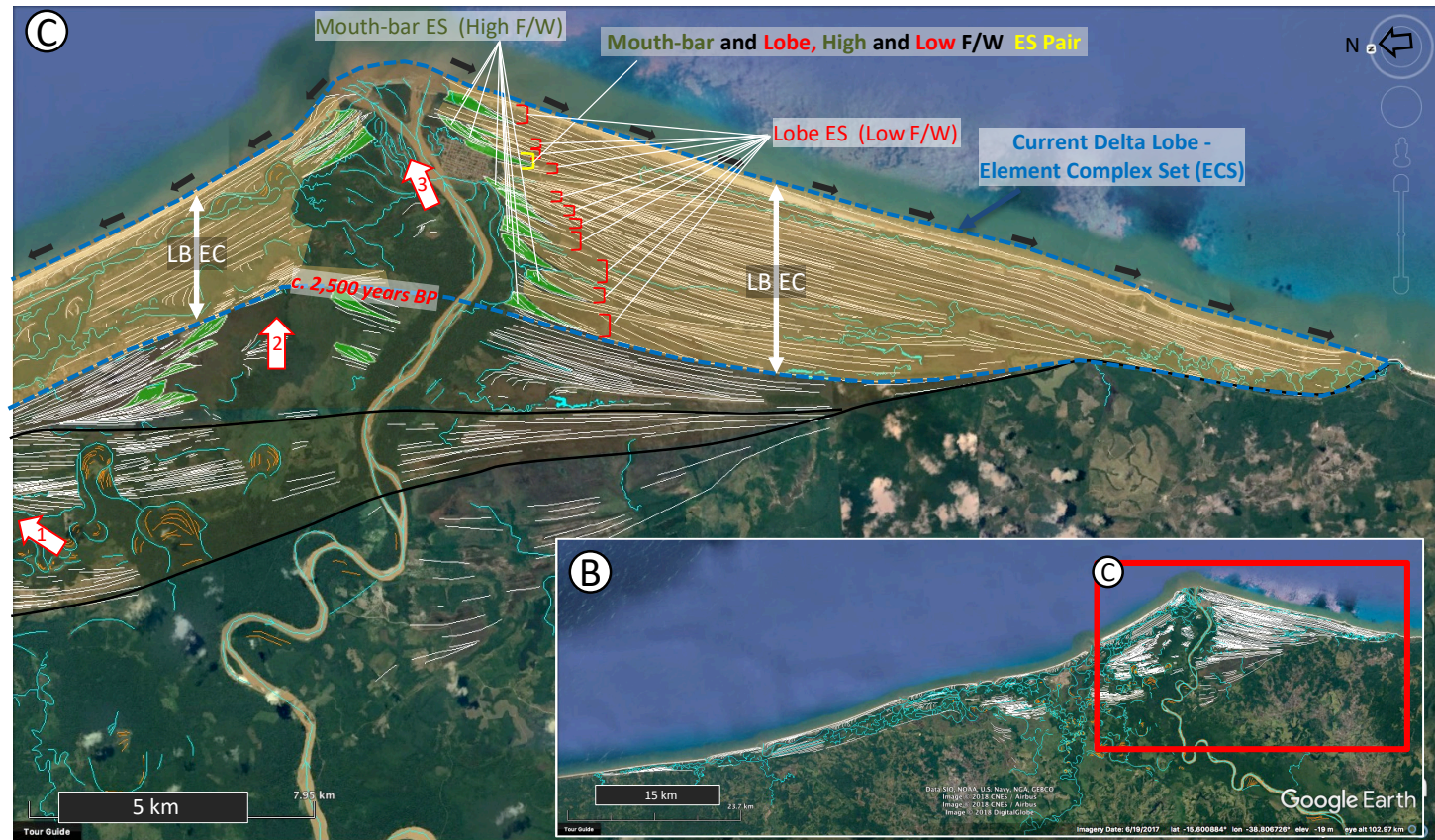
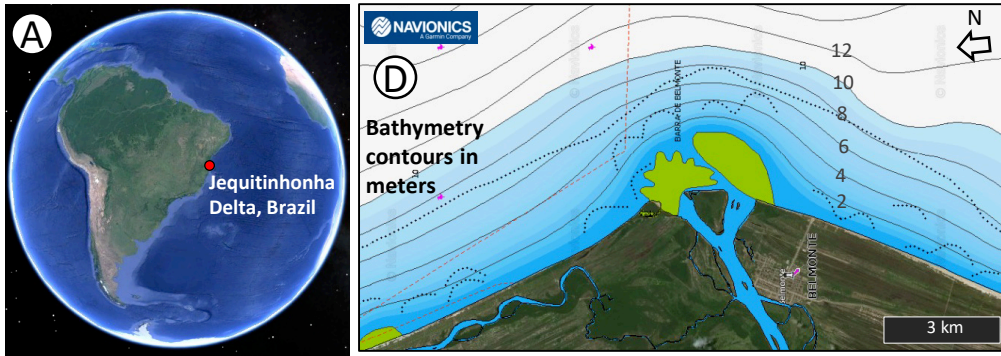


- (i) Element clinoforms: Numerous with restricted lateral extent
- (ii) Element set clinoforms: Fewer with intermediate extent
- (iii) Element-complex set clinoforms: Few with most significant lateral extent

Fig. 8



# Jequitinhonha Delta, Brazil



--- Current Element Complex Set (ECS; delta lobe) boundary / Older ECS boundary

--- Unconformity (ECS scale)

↗ ↘ Major fluvial point source depo-center (delta lobe or element complex set)

Element - Beach ridge

Element set (ES) - Beach ridge set

Centerline of watercourse

MB = Mouth bar LB = Lobe

↕ Element complex (EC)

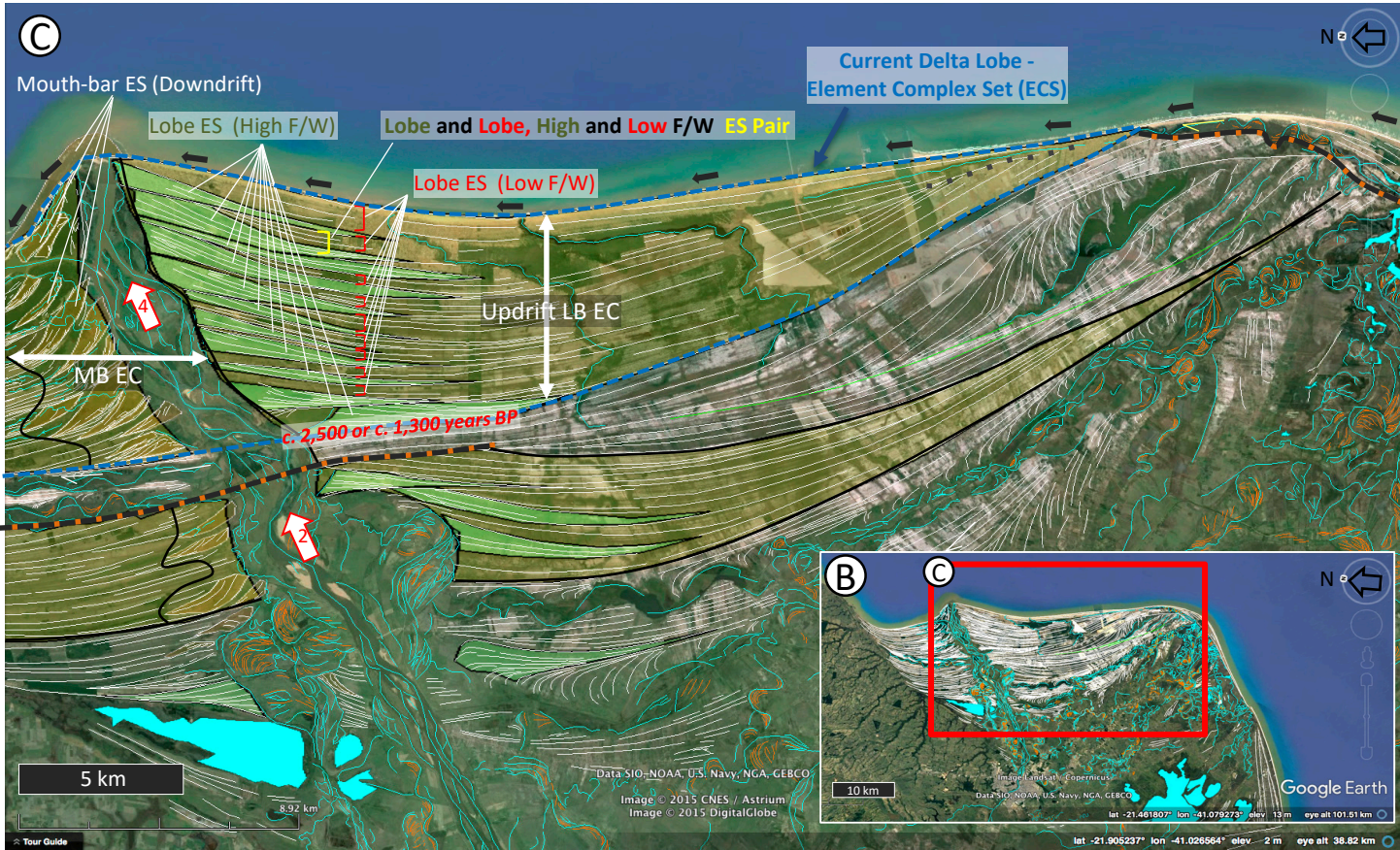
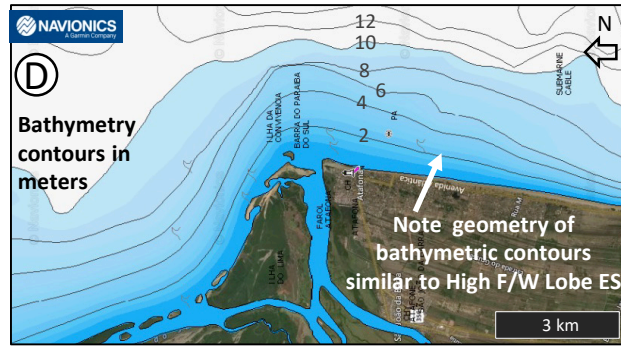
← Present day dominant longshore transport direction

ES - High F/W

ES - Low F/W



# Paraíba do Sul Delta, Brazil



--- Current Element Complex Set (ECS; delta lobe) boundary / Older ECS boundary

Element - Beach ridge

MB = Mouth bar LB = Lobe

ES - High F/W

--- Unconformity (ECS scale)

Element set (ES) - Beach ridge set

Element complex (EC)

ES - Low F/W

Major fluvial point source depo-center (delta lobe or element complex set)

Centerline of watercourse

Present day dominant longshore transport direction

Consistent and coherent plan and vertical section terms ( <i>WAVE</i> Classification)	Equivalent plan section geomorphological terms	Equivalent vertical section stratigraphic terms	Comments
Element (e.g. lobe beach-ridge element); <i>E</i>	Beach ridge	Bedset – as used in this paper (see comments)	An element is represented by a genetically related thickening or thinning-upwards set of beds. This is descriptively termed a “bedset” in this paper and by Ainsworth et al. (2016, 2017).
Element Set (e.g. lobe beach-ridge element-set); <i>ES</i>	Beach-ridge set	NA	Also termed a bedset by some authors.
Element Set Pair (e.g. mouth-bar and lobe beach-ridge element-set pair); <i>ESP</i>	NA	NA	A new term introduced in this paper.
Element Complex (e.g. lobe element-complex, mouth-bar element-complex); <i>EC</i>	Mouth bar, updrift delta, down-drift delta	Facies Association	Facies associations in low accommodation systems (c.f. Ainsworth et al. 2017) have also been described as bedsets and parasequences (when bounded by flooding surfaces) by some authors.
Element Complex Set (e.g. Wf element-complex set); <i>ECS</i>	Delta lobe	Bedset (as previously applied in the Book Cliffs; e.g. Sømme et al. 2008). Parasequence (e.g. Bhattacharya and Walker, 1991; Pattison, 1995; Van Wagoner, 1995)	Note the multiple and confusing terms used for this level of architectural hierarchy in the literature. Also note that the “equivalent” terminology shown here is for wave-dominated systems only. Fluvial-dominated systems have been called another set of “lobe” terminology by multiple authors (e.g. Frazier, 1967).
Element Complex Assemblage (e.g. Wf element-complex-assemblage set); <i>ECA</i>	Delta	Parasequence. Parasequence Set.	In wave-dominated systems, this is commonly the whole delta (e.g. the Paraiba do Sul Delta; Fig. 11).
Regressive Element Complex Assemblage Set; <i>RECAS</i>	NA	Regressive Systems Tract (5 <sup>th</sup> order). Parasequence Set.	Fifth order here represents timescales of 10 <sup>4</sup> to 10 <sup>5</sup> years.
Transgressive Element Complex Assemblage Set; <i>TECAS</i>	NA	Transgressive Systems Tract (5 <sup>th</sup> order).	Fifth order here represents timescales of 10 <sup>4</sup> to 10 <sup>5</sup> years. Represented by a transgressive lag in low accommodation systems.
Regressive-Transgressive (full or partial shelf transit) Sequence; <i>RT Sequence</i> or <i>RTS</i> .	NA	Parasequence (e.g. Mitchum and Van Wagoner, 1991; Ainsworth, 1994; Taylor and Lovell, 1995; Hampson, 2000). Fifth order, high-frequency Galloway sequence.	This level of hierarchy is the preferred level for the term “parasequence” (PS) when using the <i>WAVE</i> classification terminology (e.g. Ainsworth et al. 2018; this paper). The parasequence term is also used at this hierarchical level in the classical Book Cliffs papers (e.g. Hampson, 2000; Hampson et al. 2012).

**TABLE 1.** Comparison of *WAVE* Classification terms for both plan and vertical section stratigraphic units relevant to wave-dominated deltas (Vakarelov and Ainsworth, 2013; Ainsworth et al. 2017) with commonly used geomorphological terms for plan views and stratigraphic terms for vertical sections (see Figures 2 and 7). Note that many of the stratigraphic units have no common geomorphological term (column 2; NA = not applicable) or vertical section stratigraphic term (column 3) making correlation of plan view geometries to vertical section geometries problematical and prone to terminological misunderstandings and errors. Also note the common and confusing use of the terms “bedset”, “parasequence” and “parasequence set” at two to three different vertical hierarchical scales (columns 3 and 4). The *WAVE* Classification (column 1) provides a consistent and coherent language for comparing plan section and vertical section stratigraphic architectures. Abbreviations of *WAVE* terms are shown in *italics* at the end of the descriptions in column 1.



Delta River Mouth. Current active ECS	Delta Classification (WAVE)	Climate Zone (Koppen- Geiger)	Catchment Area (km <sup>2</sup> )	Mean Spring Tidal Range (m)	ECS Duration (Years)	ECS Progradation Distance (m)	Minimum Progradation Rate (m per year)	# of ES pairs	Duration per ES pair (Years)	Dating Method	Source
<b>Usumacinta–Grijalva (Mexico)</b>	Wf Symmetrical	Tropical Monsoon	121,025	0.3	c. 970	7,000	7.2	10	c. 97	OSL & <sup>14</sup> C	Nooren et al. (2017)
<b>Jequitinhonha (Brazil)</b>	Wf Symmetrical	Tropical Wet	70,742	2.2	c. 2,500	8,000	3.2	11	c. 227	<sup>14</sup> C	Martin et al. (1993)
<b>Paraíba do Sul (Brazil)</b>	Wf Asymmetrical	Tropical Savanna	57,085	1.3	c. 2,500	11,000	4.4	11	c. 227	<sup>14</sup> C	Martin et al. (1993)
<b>Paraíba do Sul (Brazil)</b>	Wf Asymmetrical	Tropical Savanna	57,085	1.3	c. 1,300	11,000	8.5	11	c. 118	OSL	Vasconcelos et al. (2016)

**TABLE 2.** Data for three Holocene delta lobes (element complex sets; ECS). Note the duration of element set (ES) pairs for each delta is estimated at around 100 to 200 years. Data for the Paraíba do Sul from Martin et al. (1993) and Vasconcelos et al. (2016), the Jequitinhonha delta from Martin et al. (1993), and the Usumacinta–Grijalva delta from Nooren et al. (2017). <sup>14</sup>C = Carbon 14 absolute dating methods. OSL = optically stimulated luminescence absolute dating methods. N.B. absolute age durations have an uncertainty associated with the measurements (see details in relevant sources), hence they are stated as approximate durations (c. = circa).

Architectural Unit Name	Plan View (Geomorphology)	Rock Record (Vertical Section)	Probable Timeframe	Possible Response Type and Formative Mechanism
Bed	Lobate, sub-regional, km to multi-km-scale feature.	Bed: Single mm to cm scale bed in vertical section.	Hours to days per bed, but frequency of individual storm events may be seasonal or annual (months to years).	Autogenic: Fairweather wave activity, fluvial discharge fluctuations and individual storm events.
Element (E)	Beach Ridge: Single sub-regional beach ridge, km to multi-km-scale.	Bedset: A group of genetically related beds that can be arranged in an upward-thickening or upward-thinning trend. (decimeter- to meter-scale).	10s to 100s of years	Autogenic: Large (once in a decade-scale) storms can initiate new ridges. Fairweather and regular storm-related bed deposition are also part of the formative process. Mouth-bar unloading events may trigger new element formation?
Element Set (ES)	Beach Ridge Set: Multiple, grouped beach-ridges. Sub-regional, multi-km scale.	A group of genetically related bedsets (elements): Dominant normal progradation mode promotes vertical stacking of elements in offshore locations (meter scale).	10s to 100s of years	Allogenic: Part of a centennial-scale climate cycle influencing F/W at the coastline by changing river catchment precipitation and hence fluvial discharge, and/or wave power. The ES is either low or high F/W.
Element Set Pair	Two grouped beach ridge sets bounded by a disconformity or discontinuity. Sub-regional, multi-km scale.	A pair of genetically related element sets: Dominant normal progradation mode promotes lateral offset stacking of element set pairs in offshore locations (meter scale).	100s of years	Allogenic: A full centennial-scale climate cycle of high to low F/W at the coastline which alters river catchment precipitation and hence fluvial discharge, and/or wave power.
Element Complex Set (ECS)	Delta Lobe. Sub-regional, multi-km scale.	A group of genetically related element sets, element set pairs and element complexes (meter to decameter scale).	100s to 1000s of years	Autogenic: One river avulsion event on the delta plain.

**TABLE 3.** Description, probable timeframe of deposition, response type and formative mechanism for architectural units on wave-dominated deltas.